

Ferroelectric Thin Films for Oxide Electronics

Review Article

Author(s):

Müller, Marvin; Efe, Ipek ; Sarott, Martin F. ; Gradauskaite, Elzbieta ; Trassin, Morgan 

Publication date:

2023-03-28

Permanent link:

<https://doi.org/https://doi.org/10.3929/ethz-b-000602179>

Rights / license:

[In Copyright - Non-Commercial Use Permitted](#)

Originally published in:

ACS Applied Electronic Materials 5(3), <https://doi.org/10.1021/acsaelm.2c01755>

Funding acknowledgement:

- Multifunctional oxide electronics using natural ferroelectric superlattices ()
- Designing oxide electronics with light ()

Ferroelectric thin films for oxide electronics

Marvin Müller*, Ipek Efe, Martin F. Sarott, Elzbieta Gradauskaite and
Morgan Trassin*

Department of Materials, ETH Zurich, Zurich 8093, Switzerland

E-mail: marvin.mueller@mat.ethz.ch; morgan.trassin@mat.ethz.ch

Abstract: Ferroelectric materials have set in motion numerous ultralow-energy-consuming device concepts that can be integrated into state-of-the-art complementary metal–oxide–semiconductor technology. Their non-volatile, spontaneous electric polarization makes them promising candidates to control functionalities at the nanoscale with energy-efficient electric fields only. In this spotlight article, we start with a brief introduction to ferroelectric materials, the challenges involving the design of thin films, and review the state-of-the-art of their integration into various electronic applications. Revolutionary in-situ and operando diagnostic tools allowing the monitoring of the technology-relevant polarization state during the material design, or its operation will be detailed. Concepts such as chiral states in ferroelectrics and neuromorphic-type switching will be addressed to provide a comprehensive view on the evolution of ferroelectric states for the next generation of low energy-consuming electronics. Finally, we discuss the most recent developments in the field, including the emergence of ferroelectricity at the nanoscale and in two-dimensional systems.

Keywords: ferroelectrics, oxides, thin films, beyond-CMOS, second-harmonic generation, operando SHG, in-situ SHG, perovskites

1. INTRODUCTION

With this spotlight article, we aim to give an overview of the recent developments in the characterization of ferroelectric materials, described by their spontaneous electrical polarization that can be reversibly and remanently manipulated by an external electric field. This polarization results in an accumulation of bound charges at the surfaces of the material and is measured in charge per unit area, most commonly in $\mu\text{C}/\text{cm}^2$. There are several microscopic mechanisms that describe the emergence of a spontaneous electric polarization in oxide materials. In section 1, we describe these mechanisms with a particular emphasis on the potential of ferroelectric materials for energy-efficient oxide electronics, including a discussion on the challenges accompanying the downscaling of ferroelectric thin-films for nanoscale device integration. Then we will move on to the description of the most recent device concepts involving ferroelectrics for low energy-consuming operation in section 2. In section 3, we cover the recent developments in advanced characterization tools for the successful integration of ferroelectric films into technological devices. Here, we put our focus on the in-situ and operando investigation of ferroelectric states at the nanoscale. In section 4, the state-of-the-art approaches to stabilize a robust polarization in the ultrathin regime will be detailed. Finally, in section 5, we discuss future perspectives and presently emerging ferroelectric concepts and materials systems, such as the electric counterpart of the magnetic Dzyaloshinskii-Moriya interaction and ferroelectricity in two-dimensional (2D) materials.

1.1. Conditions for the emergence of a ferroelectric polarization

In the prototypical ABO_3 perovskite structure, the symmetry of the unit cell is determined by the relative sizes of the A and B cations positioned at the corners and the center of the oxygen octahedral cage, respectively. For B -site cations with a sufficiently small radius and an electronic configuration of d_0 -type, a spontaneous displacement away from the center of the oxygen octahedral cage can be stabilized by an orbital hybridization with the $2p$ orbitals of the oxygen anion. This results in the formation of a stable electric dipole within each perovskite unit cell that will sum up to a macroscopic polarization in the material if long-range ordering takes place. This type of ferroelectricity – referred to as B -driven ferroelectricity (see Figure 1a) – corresponds to the most common mechanism and is observed in prototypical systems such as $BaTiO_3$, $PbTiO_3$, and $Pb[Zr_xTi_{1-x}]O_3$.¹ In this case, the symmetry of the unit cell changes from cubic to tetragonal across the ferroelectric phase transition. Hence, six different ferroelectric domain variants can emerge, as the electrical dipole within the perovskite unit cell can point towards any of the six faces of the formerly cubic unit cell. At the same time, the onset of the polarization leads to a structural distortion, thus, resulting in a strong lattice-polarization coupling in ferroelectric materials.² For further reading on electromechanical applications of ferroelectrics and the piezoelectric effect, i.e. the lattice deformation leading to a voltage buildup in the material, we refer the reader to the reviews by Rödel *et al.*³ and Setter *et al.*⁴ B -driven ferroelectricity is not the only mechanism leading to an onset of an electric dipole within a unit cell.⁵ When the A -site cation possesses an electronic configuration with a lone pair, the electron cloud of this non-bonding lone pair can spontaneously distort the oxygen octahedron. This stereochemical activity, depicted in Figure 1b, then leads to a ferroelectric polarization pointing along any of the cubic diagonal directions of the perovskite unit cell. The so-called A -driven ferroelectricity is the dominant mechanism that drives the onset of ferroelectricity in the compound $BiFeO_3$ ⁵ and also contributes to the polarization of $Pb[Zr_xTi_{1-x}]O_3$ -based compounds. Apart from B - and A -driven ferroelectricity, where the polarization is the primary order parameter, it can also occur that the polarization itself is not the main order parameter across the phase transition. In geometric ferroelectrics, such as the hexagonal manganites, with $YMnO_3$ as a model system, the driving force across the transition is a rotational instability of the MnO_5 polyhedra, which triggers a displacement of the A -site cation, and result in a so-called lattice trimerization.⁶ The MnO_5 bipyramids can buckle in or out and enforce an A -cation displacement upwards or downwards with respect to the long axis of the hexagonal unit cell, see Figure 1c. The resulting cation rearrangement, hence, induces a polarization which points along the c -axis of the hexagonal unit cell. It is worth pointing out that this unconventional origin for ferroelectricity, often referred to as improper ferroelectricity, leads to exotic domain architectures since, at the phase transition, the polarization configuration at the domain boundaries is not bound to the classical rules of electrostatics. Charged head-to-head and tail-to-tail domain walls are routinely observed in such geometric ferroelectrics that would be energetically unfavorable in proper ferroelectrics.⁷ Finally, a net polarization can be triggered by the spatial ordering of charges in a non-centrosymmetric arrangement, as in the case of charge-ordered ferroelectrics. Figure 1d represents the superpositions of Fe^{2+} -based and Fe^{3+} -based layers and the corresponding polarization in the compound $LuFe_2O_3$.⁵

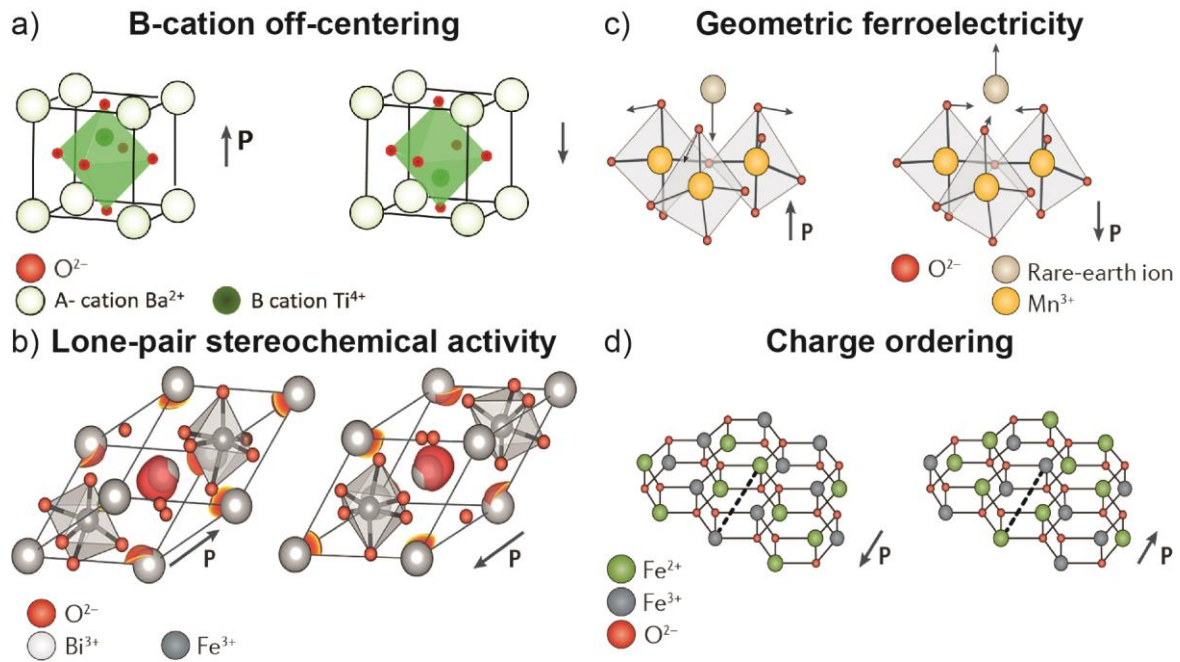


Figure 1: Microscopic origin of ferroelectricity. a) Ferroelectricity driven by the B-cation off-centering for the case of BaTiO_3 . b) A-driven ferroelectricity that is driven by the stereochemical activity of the A-cation lone-pair for the example of BiFeO_3 . Reproduced with permission from ⁵, copyright 2016 by Macmillan Publishers. c) Ferroelectricity induced by a purely geometrical distortion. Here, in the case of RMnO_3 , the tilting of the MnO_5 bipyramids causes a polar displacement of the rare-earth R^{3+} ion. Reproduced with permission from ⁵, copyright 2016 by Macmillan Publishers. d) In charge-ordered ferroelectrics a non-centrosymmetric arrangement of charge can give rise to a non-zero polarization. Here, it's shown for the case of LuFe_2O_3 which forms alternating layers with $\text{Fe}^{2+}/\text{Fe}^{3+}$ ratios of 2:1 and 1:2, which create a spontaneous polarization along the dashed line and solid arrow. Reproduced with permission from ⁵, copyright (2016) by Macmillan Publishers.

1.2. Ferroelectric behavior in technologically relevant thin films

The key challenge for the integration of ferroelectric thin-films into electronic devices consists in preserving the ferroelectric behavior in the ultrathin (down to a few unit cells) regime.⁸ The emergence of the ferroelectric polarization, however, induces the accumulation of bound charges at the surface of the films. In return, these charges create an electric field oriented oppositely to the polarization and in the ultrathin regime, the contribution of this so-called depolarization field dominates and suppresses the net polarization.^{9–11} Additionally, in epitaxial heterostructures, the substrate interface can mechanically clamp the structure of the ferroelectric material and thus present another source of polarization suppression, as in the case of geometrically driven improper ferroelectrics.¹² Figures 2a and 2b represent the typical loss of tetragonality accompanying the polarization suppression as the thickness is reduced in PbTiO_3 films, as well as the critical thickness observed in epitaxial improper ferroelectric YMnO_3 thin-films due to the substrate clamping effect, respectively.^{12,13} The current approach undertaken by the community to combat the detrimental effects of the depolarization field in B-driven ferroelectrics takes advantage of the strong lattice-polarization coupling in such films.^{2,8} Specifically, the polarization amplitude of the film can be drastically influenced by a lattice deformation induced by epitaxial strain,^{9,14} see Figure 2c.¹⁵ Thus, in order to boost the technologically relevant out-of-plane-oriented ferroelectric polarization in thin films, the polar distortions and lattice tetragonality are enforced using single crystalline substrates that provide compressive strain in the

epitaxial thin film design, as schematized in the Figure 2d. The selection of adequate substrates became key in the stabilization of ferroelectricity in the ultrathin regime, and a non-vanishing polarization has been reported down to a film thickness of only 4 unit cells.⁹ The ability to transfer these epitaxial strain states onto the silicon platform using SrTiO₃ buffered silicon wafers renders the epitaxial deposition of ferroelectric films of extremely high relevance for technological applications.^{16–18}

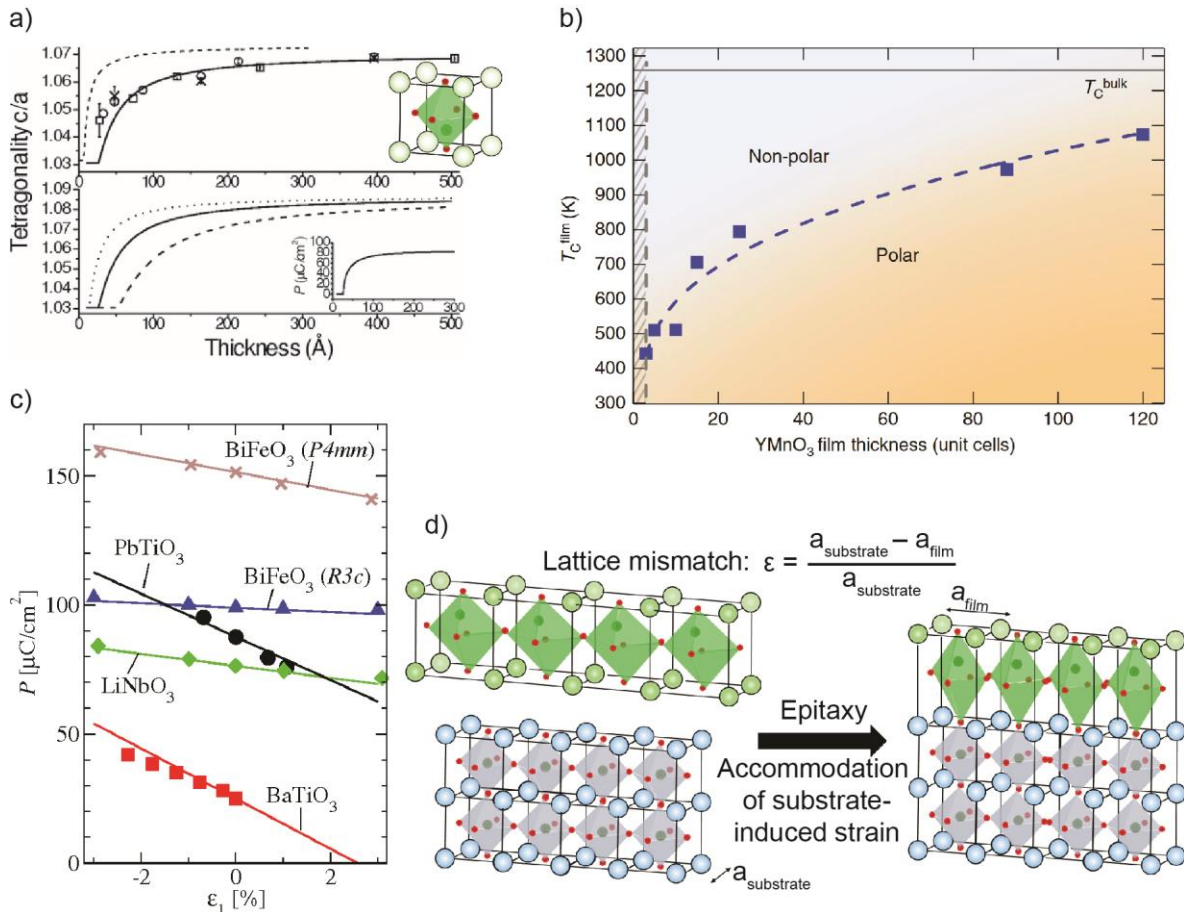


Figure 2: Limits of ferroelectricity due to size effects. a) Loss of tetragonality and the concurrent polarization in PbTiO₃ thin-films at reduced thicknesses. Reproduced with permission from ¹³, copyright (2005) by the American Physical Society. b) Observation of critical thickness in improper YMnO₃ films due to substrate clamping. Reproduced with permission from ¹², copyright (2019) by the Nature Publishing Group. c) Influence of epitaxial strain on the ferroelectric polarization magnitude for a set of prototypical ferroelectrics. Reproduced with permission from ¹⁵, copyright (2005) by the American Physical Society. d) Deformation of the unit cell of BaTiO₃ when it is epitaxially grown under compressive strain on a substrate with smaller in-plane lattice constants.

The understanding and control of the microscopic mechanisms leading to the emergence of ferroelectricity and the strong correlation between the lattice strain and the polarization state is key to stabilize robust polarization states in the ultrathin regime. While the epitaxial design of high-quality thin-films stands out as the most promising way to engineer ferroelectricity in the thin film form, the selection of non-perovskite systems in which the polarization emerges at the nanoscale only, such as hafnia-based compounds and 2D ferroelectrics, emerge as promising alternatives. In parallel, means to characterize polarization states in the technologically relevant ultrathin regime are constantly improving. The next section will highlight the emerging device paradigms that have ferroelectric thin-films integrated into their architecture.

2. FERROELECTRICS FOR OXIDE ELECTRONICS: STATE-OF-THE-ART AND CURRENT LIMITATIONS

2.1 Energy-efficient oxide electronics

The pervasive need for device miniaturization brings the complementary metal–oxide–semiconductor (CMOS) technology to its fundamental limits. In particular, the Boltzmann tyranny which describes the fundamental limit in the energy cost of a logic operation imposes severe restrictions on the further development.^{19,20} In the standard field-effect transistor (FET) architecture, this translates to a minimal voltage required to change the source-to-drain current by one order of magnitude. The limit of this subthreshold swing has been identified as 60 mV/decade. This puts extreme constraints on the materials properties. Eventually, the miniaturization and the concomitant power density increase call for a device paradigm shift towards energy-efficient and scalable memory, information storage, and processing devices beyond solely performance-driven innovations. Complex transition metal oxides span a wide range of functionalities, and in thin-film form, their foreseen applications hold promise to revolutionize the CMOS technology. For instance, oxides can exhibit ferromagnetic and ferroelectric behavior, which are relevant for technological applications in non-volatile data storage.^{5,21,22} The net ferroelectric polarization is highly attractive for memory devices and logic operation applications because it can be manipulated solely with electric fields.²³ Thus, in contrast to their magnetic counterparts, which necessitate highly energy-consuming magnetic fields or high-density spin-polarized currents to set a desired magnetic state, the use of ferroelectric materials may enable the control of data storage devices with limited energy dissipation. Here, the origin of Joule heating resides mainly in the material-dependent dielectric, mechanical, and electromechanical losses²⁴ associated with the hysteretic nature of the polarization switching process²⁵. We note that the investigation of such heat dissipation processes in nanoscale ferroelectric-based devices are still underexplored. Increasing the energy efficiency and scalability of such oxide-based electronics would lastingly reduce CO₂ emissions and slow down global warming. The ultralow energy consumption of such computing chips would also support the upcoming revolution of the internet-of-things that relies on integrated batteries and power sources. In the following, we will describe the basic concepts of the most prominent ferroelectrics-based device designs.

2.2. Ferroelectric field-effect transistors

In modern metal-oxide-semiconductor field-effect transistors (MOSFETs) the electron flow from source to drain is controlled by a voltage applied to the gate. The gate metal is separated from the conduction channel by a dielectric oxide and the gate voltage generates an electric field which penetrates the Si channel controlling the charge carrier density. This enables the control of the source-to-drain conductance and thus, of the transistor state. The main limitation of the FET resides in the volatility of the conductance state. Once the gate voltage is removed, the charge accumulation at the interface with the channel is lost. Recently, this issue was successfully resolved through the substitution of the high- κ dielectric gate material with a ferroelectric material as depicted schematically for a transistor in Figure 3a. The unscreened bound charges accompanying the remanent ferroelectric polarization generate a non-volatile

electric field to the Si channel. Switching of the polarization using a voltage pulse reverses the static electric field from the bound charges and can thus switch the state of the transistor remanently. Non-volatile ferroelectric field-effect transistor (FeFET) prototypes were already built, optimized, and benchmarked. The current design integrating ferroelectric gate materials such as zirconium-doped HfO₂ shows promising performance and exhibits improved energy efficiency and faster operation than dynamic random-access memories (DRAMs) or static RAMs (SRAMs).²⁶ For further reading, the authors recommend the recent review by Kim *et al.*²⁶.

2.3. Negative capacitance FET

The theoretical concept of negative capacitance (NC) roots back to the late 1970s²⁷. Its incorporation into the FET design for reduced energy consumption has, however, not been suggested until 2008²⁰. In the following, we will give a brief and intuitive explanation of the emergence and application of the NC effect for the advanced ferroelectric FET architecture. For further reading, we can recommend the excellent review by Saha *et al.*²⁸. In practice, the NC-FET relies on a ferroelectric/dielectric bilayer as gate material. The dielectric layer does not screen the bound charges accumulating at the ferroelectric interface and, as a consequence, a strong depolarizing field suppresses the net polarization in the ferroelectric gate material, forcing it into an incipient ferroelectric (IFE) state. The application of an external voltage at the gate triggers a sudden ferroelectric transition from the incipient state. As depicted in Figure 3b, the corresponding abrupt increase of bound charge accumulation sums up with the voltage supply-induced charge accumulation. Thus, the charge accumulation across the dielectric exceeds the one supplied by the external voltage, leading to the voltage amplification at the gate. The NC-FET, hence, offers avenues to breach the limitations imposed by the Boltzmann tyranny on conventional CMOS technology. Experimental demonstrations of the negative capacitance effect first involved typical perovskite heterostructures like PbTiO₃/SrTiO₃.²⁹ Recently, architectures with CMOS-compatible HfO₂-based materials have been reported.³⁰

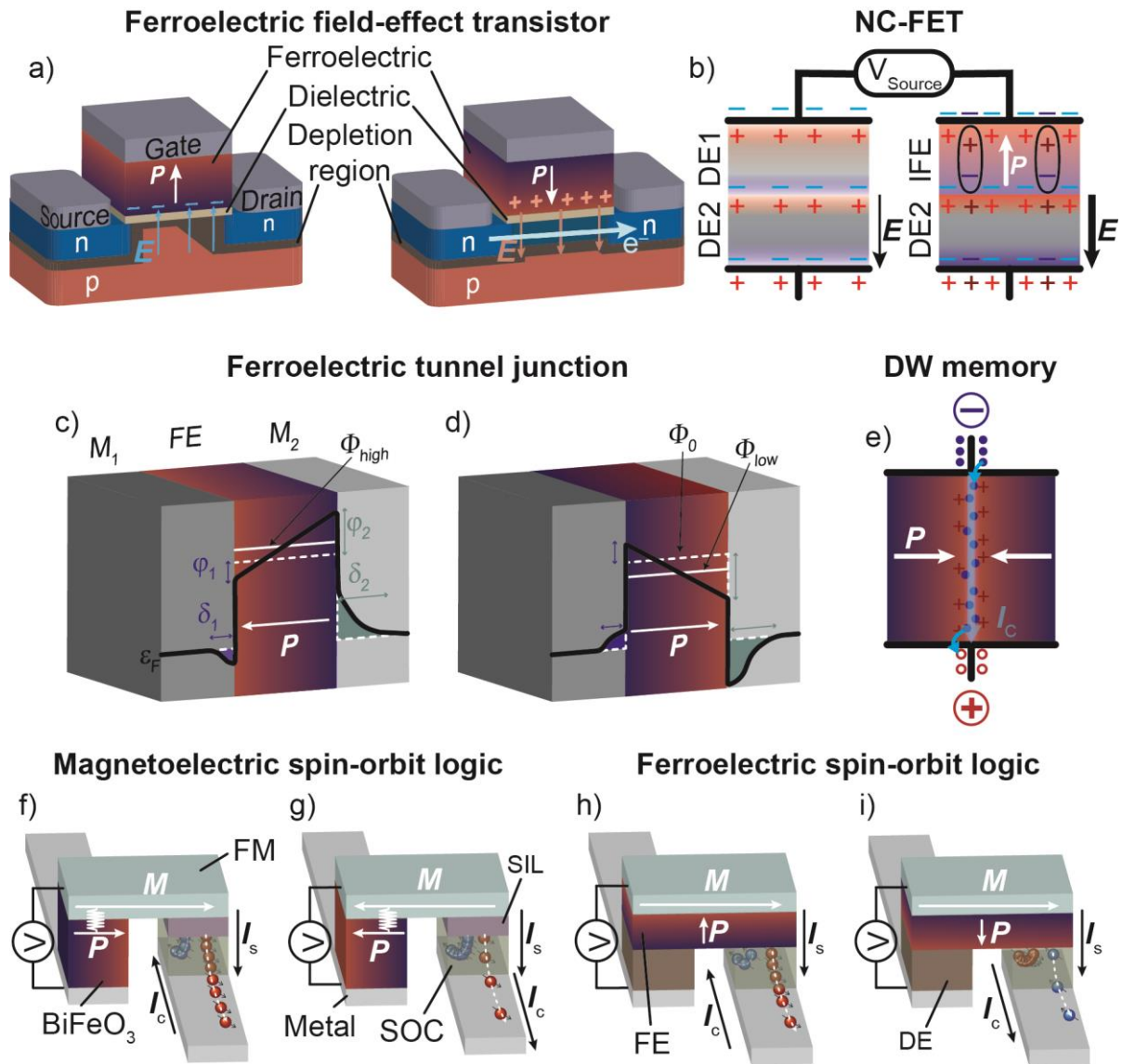


Figure 3: Device concepts based on ferroelectrics. a) Working principle of a ferroelectric field-effect transistor. b) Schematic illustration of the voltage amplification due to the negative capacitance effect. The bright-colored charges represent the charges from the voltage source and the dark-colored charges represent the additional charges originating from the onset of ferroelectric polarization from the incipient ferroelectric state. c), d) Dependence of the ferroelectric polarization direction on the tunnel-barrier height in a ferroelectric tunnel junction e) Schematic illustration of a domain wall memory. The conductance is confined to a charged domain-wall channel. Here, the plus signs correspond to bound charges arising from the polarization, and the blue dots and red circles represent free electrons and holes, respectively. f), g) Magnetoelectric spin-orbit logic devices. The net in-plane polarization of the magnetoelectric multiferroic sets the magnetization in the adjacent ferromagnetic (FM) layer. At the read-out node, the spin-polarized current I_s from the FM is injected into a layer with strong spin-orbit coupling (SOC) through a spin-injection layer (SIL). The spin-to-charge conversion eventually leads to a detectable charge current I_c . h), i) Ferroelectric spin-orbit logic devices. The application of a voltage to the writing node switches the polarization in the ferroelectric (FE). The read-out is based on the injection of a spin current from the ferromagnet into a SOC layer. The spin-to-charge conversion and hence, the I_c , depends on the polarization state of the FE.

2.4. Ferroelectric tunnel junctions and electric-field controllable memristive behavior

The ferroelectric tunnel junction (FTJ) architecture consists of a ferroelectric material sandwiched in a parallel-plate capacitor geometry between two different metallic electrodes, see Figure 3c, 3d. If the thickness of the ferroelectric film is reduced to a few nanometers, finite quantum-mechanical tunneling through the ferroelectric material

becomes possible. The difference in the metallic screening lengths δ in the metal electrodes $M_{1,2}$ for the bound charges of the ferroelectric material results in an asymmetric tunneling potential and thus in a tunnel barrier height Φ which depends on the polarization direction. In other words, the resistance across the FTJ and therefore the state of a bit can be read non-destructively and set simply by switching the ferroelectric polarization.³¹ In addition, the application of sub-coercive-field voltage pulses, which trigger incomplete switching of the ferroelectric polarization enable macroscopic polarization states beyond the two saturation states and therefore the continuous tuning of the tunneling electroresistance of the FTJ. Consequently, a memristive behavior, originally developed in the resistive RAM design, has been developed in BaTiO₃-based systems.³² We emphasize here that the memristive behavior is key in the design of neuromorphic-type computing schemes, in which more than two remanent states are necessary per computing bits. We recommend the excellent reviews by Zidan *et al.*³³, and Asif *et al.*³² for an overview over the state-of-the-art design of memristors and the review by Garcia *et al.*³⁴ for the latest insights into FTJs.

2.5. Ferroelectric domain-wall nanoelectronics

The seminal demonstration of local conductance at ferroelectric domain walls in BiFeO₃ films triggered an immense interest in the scientific community.³⁵ In ferroelectric materials, the electrostatic boundary conditions most commonly drive the domain and domain-wall formation. Thus, bound charge accumulation is usually minimized at the domain walls. If the polarization configuration at the wall deviates from this neutral configuration, however, the necessity to screen the resulting bound charge accumulation will drive the attraction of free charge carriers or charged defects and can, hence, drastically alter the local transport properties at the domain wall.^{36,37} The search for means to stabilize so-called charged domain walls exhibiting a head-to-head or tail-to-tail polarization configuration and the exploration of improper ferroelectric materials, in which charged domain walls can spontaneously form, led to the expansion of the field. Because ferroelectric domain walls can be nucleated, erased, and moved at will using electric-field application, the potential of rewritable nanocircuitry and domain-wall memory cells rapidly emerged. The most straightforward application of charged domain walls is a ferroelectric domain-wall memory cell which is based on a parallel-plate capacitor structure encapsulating a ferroelectric material, similar to the device concept of the FTJ. Here, conduction through the capacitor is enabled through the localized charge carrier mobility at the ferroelectric domain walls, as depicted in Figure 3e. Most advanced architectures involve BiFeO₃ thin films and hexagonal manganites.³⁵ Neuromorphic plasticity in such domain-wall-based devices is established through the control over the number of charged domain walls in the device. For a more extensive description of the physics and the possible applications arising from ferroelectric domain walls, the reader is referred to the review by Meier *et al.*³⁸.

2.6. Magnetoelectric and ferroelectric spin-orbit logic devices

The writing process in the magnetoelectric spin-orbit (MESO) device¹⁹ is based on the integration of multiferroic magnetoelectric materials into scalable spintronic logic devices. Such materials exhibiting coexisting and coupled ferroelectric and ferromagnetic long-range order would enable the conversion of an electric input into a

magnetization change via the magnetoelectric effect.^{21,22} Motivated by the demonstration of the reversal of a net magnetization using an electric field in heterostructures based on magnetoelectric BiFeO₃ at room temperature, the MESO device promises ultra-low energy consuming writing operation of magnetic bits.¹⁹ While the magnetoelectric coupling enables the writing of the magnetic information into the ferromagnetic layer, the read-out involves either the inverse spin-Hall or Edelstein effect which transduces a spin state into a measurable charge current. As depicted in Figures 3f and 3g, in the simplest geometry, the ferromagnetic layer is connected to a metal with strong spin-orbit coupling. A major advantage of such a device architecture is that the MESO nodes can be cascaded as the charge current output can be used as input in the next MESO structure. This brings the potential to improve the energy efficiency and performance by overcoming the von Neumann bottleneck with in-memory computing.^{19,33} Recently, ferroelectric control over the spin-to-charge conversion via the inverse Edelstein effect was demonstrated in GeTe and SrTiO₃-based designs.³⁹ The ability to use the ferroelectric polarization state as a means to control the voltage read-out gave rise to a similar device concept that relies solely on the ferroelectric properties, instead of the magnetoelectric properties, see Figures 3h and 3i. Such a ferroelectric spin-orbit logic device promises similar non-volatile data storage and in-memory computing functionalities without the need to store the data in the magnetic layer.

2.7. Towards the successful integration of ferroelectric thin films in nanoscale devices

All these device concepts hold promises for highly efficient oxide electronics and suggest ferroelectrics-based device architectures as realistic additions to the existing silicon-based technology. The actual integration of such devices, however, relies on an improved understanding of the ferroelectric states at the nanoscale, where interfaces and electrostatic boundary conditions dominate the final polarization state. As we described above, the emergence of the depolarizing field imposes severe difficulties on the design of materials with substantial ferroelectricity at the nanoscale. It even persists in a metal/ferroelectric/metal capacitor geometry, and therefore hinders the integration of ultrathin ferroelectrics into technological devices, due to the limited screening length of metallic electrodes.⁴⁰ Other factors such the abovementioned heat dissipation due to losses in ferroelectrics and increased current densities in tunneling devices underline the need for further investigations in the ultrathin regime. Hence, the ability to identify novel ways to manipulate, control, and eventually exploit the depolarizing field during the fabrication of ferroelectric devices motivates the in-situ investigation of polarization states in thin films during the growth. While recent studies and review articles have provided detailed descriptions of ferroelectric characterization tools^{2,41–43} and because the device design necessitates the capping of ferroelectric layers, in this spotlight article, we will cover most recent approaches dealing with the determination of buried ferroelectric states and focus on in-situ, operando-compatible techniques.⁴⁴

2.8. Materials considerations

The integration of ferroelectric materials into application-relevant and CMOS-compatible device architectures puts constraints to the material selection. A critical parameter is the temperature needed for the insertion of functional ferroelectric layers.

To be compatible with the back-end-of-the-line (BEOL) processing steps, during which the interconnects are formed, processing temperatures must be kept below 400 °C.⁴⁵ Hence, tetragonal ferroelectrics such as BaTiO₃, which can be epitaxially integrated onto the silicon platform only at high temperatures, do not, at present, fulfill the requirement for integration into advanced CMOS-compatible heterostructures. Until their processing temperature is sufficiently lowered, e.g. through the development of atomic layer deposition-based processes, they remain model systems for the understanding and further development of ferroelectrics-based devices and lay down a roadmap for the optimization of BEOL-compatible ferroelectric systems.²⁶ The recent discovery of ferroelectricity in CMOS-compatible binary oxides such as HfO₂-based materials and wurtzite ferroelectrics makes these materials ideal candidate for the insertion of ferroelectric functionalities into integrated electronics. We recommend the review by Mikolajick *et al.*⁴⁶ for a detailed reading on the applicability of the next generation of ferroelectric materials. In particular, the persistence of polarization in the ultrathin regime and, compared to wurtzite materials, the low electric coercive field in HfO₂-based materials puts the binary oxides in the forefront for integration into application-relevant devices. The case of HfO₂-based thin films will be discussed in section 5.2. The main focus of this spotlight article, is, however, on the general advances in the understanding of ferroelectricity in the ultrathin regime taking established epitaxial oxide thin films as model system.

3. FERROELECTRICITY IN THE ULTRATHIN REGIME: ADVANCED CHARACTERIZATION TOOLS

The device integration of ferroelectrics most commonly involves a parallel-plate capacitor design. This geometry allows for the application of uniform electric fields across the thickness of the films to manipulate the polarization. While the macroscopic polarization can be measured along the electric field direction in such a geometry by detection of the electrical switching current via the positive-up-negative-down technique (PUND), the detailed domain architecture of the films remains inaccessible by conventional techniques. This limits our understanding of the evolution of the ferroelectric behavior as the thickness reaches the ultrathin regime and hence, hinders the integration of films with controlled polarization states into devices. To visualize the microscopic ferroelectric domain configuration, piezoresponse force microscopy (PFM) is the most convenient technique. Once the films are buried under a highly conducting electrode or complex dielectric/metallic heterostructures, however, the efficiency of PFM to spatially resolve both the in-plane and out-of-plane polarized domain architecture is reduced, since the top electrode may prevent the local readout from the scanning-probe tip.^{47,48} Hence, here, we will focus on experimental approaches giving access to buried ferroelectric states, starting with destructive approaches. We will then put the emphasis on a non-destructive and non-invasive optical characterization technique. Because of its probing depth and long working distance, the latter, namely optical second-harmonic generation (SHG), is furthermore compatible with operando characterization and is even used in-situ, during the epitaxial deposition of ferroelectric films.

3.1. Invasive characterization of integrated ferroelectric thin-films

We start with invasive tomographic atomic force microscopy (AFM) and PFM characterization, which provides information on the domain architecture throughout the volume of the film, even once integrated into a capacitor structure. Next, we highlight recent developments dealing with atom probe tomography (APT) investigations of ferroelectric materials, which, for instance, enable the chemical investigation of defect accumulations at ferroelectric domain walls.

Tomographic AFM and PFM – To address the above mentioned limitations that PFM is subject to, and in order to spatially resolve ferroelectric domains within the volume of a film or capacitor heterostructure, several tomographic techniques have been developed, including optical tomography, X-ray computed tomography, and SEM imaging with sequential FIB sectioning. Since these methods either show an optically limited resolution or require highly specialized equipment, we highlight here recent results that were obtained via subtractive tomographic AFM (T-AFM)⁴⁹. A substantial force (few μN) is locally applied to the film via the AFM tip to mechanically remove material⁵⁰, during or after which images in the selected measurement modes can be acquired, for example conducting AFM (C-AFM) or PFM⁵¹. Following this procedure, a series of 2D images are acquired that can be used to reconstruct the three-dimensional property map of the sample with very high lateral (<50 nm) and depth (<1 nm) resolution. An important experimental consideration for this approach is the minimization of sample damage underneath the surface during tip milling, which is crucial to maintain quantitative tomographic datasets. So far, the combination of T-AFM and PFM to investigate ferroelectrics has only been utilized in a couple of studies^{10,51}. In 2019, Steffes *et al.*⁵¹ achieved the first three-dimensional PFM datasets to visualize the domain configuration throughout the film thickness of stripe BiFeO_3 films grown on $\text{SrRuO}_3/\text{DyScO}_3$. In addition to confirming the inclined structure of the 71° domain walls, as previously observed with scanning transmission electron microscopy (STEM), they further showed that the thickness dependence of the spontaneous polarization and the coercive field agree with the phenomenological Landau-Ginzburg-Devonshire theory and the Kay-Dunn law. This tomographic approach further proved to be powerful to investigate the domain architecture of a buried ferroelectric layer within a parallel plate capacitor. In a stack consisting of $\text{SrRuO}_3/\text{BaTiO}_3/\text{SrRuO}_3$, nanomachining the top SrRuO_3 electrode allowed PFM imaging of the domain structure of the buried BaTiO_3 layer¹⁰, see Figures 4a–4c. The exposed BaTiO_3 revealed the formation of nanometer-scale ferroelectric domains. This work further highlighted the detrimental impact of the depolarizing field in the ultrathin regime and provided insights into means to maintain the ferroelectric behavior in ultrathin BaTiO_3 films integrated into capacitor heterostructures.

Atom probe tomography – APT is an experimental technique that enables the analysis of the three-dimensional atomic arrangement in a needle-shaped specimen with extremely high chemical sensitivity (ppm) and spatial resolution (<1 nm)^{52,53}, see Figures 4d–4f. In the so-called local electrode atom probe (LEAP) geometry, a DC electric field just below the threshold for field emission is applied between the needle specimen and a local electrode. At the location of the tip apex with radius below 100 nm, the electric field strength is significantly enhanced, such that the application of either a superimposed voltage pulse or an ultrafast laser pulse triggers field evaporation and ionization. The field-emitted ions are subsequently accelerated

towards a position-sensitive detector, providing the XY coordinate of the emitted ion in the specimen. The full three-dimensional position can then be reconstructed by taking into account the flight trajectory and the precise timing of field evaporation which is controlled by the voltage or laser pulse. The element specificity is obtained via the integration of a time-of-flight mass spectrometer that can precisely quantify the mass-to-charge ratio of the emitted ions. Ionization using voltage pulses requires the sample material to exhibit a high electrical conductivity, which restricts this operation mode to metals and highly doped semiconductors. Only with the rather recent emergence of laser-assisted APT⁵⁴ essentially all materials classes – including insulators and complex oxides⁵⁵ – have become accessible. The first studies dealing with ferroelectric systems have been reported recently.^{53,56} The high chemical sensitivity of the APT provided insights in the cation segregation of $\text{PbZr}_{0.53}\text{Ti}_{0.47}\text{O}_3$ ceramics near the morphotropic phase composition.⁵³ More recently, APT was applied to epitaxial ferroelectric Aurivillius thin-films to elucidate the three-dimensional structure of out-of-phase boundaries, driving the in-plane-polarized domain formation in the films⁵⁶, as depicted in Figures 4g–4i. Furthermore, in the doped ferroelectric hexagonal manganite $\text{Er}(\text{Mn},\text{Ti})\text{O}_3$ it was possible to map the position of the Ti dopants despite their extremely low concentration of 0.04 at%.⁵⁷ Understanding the distribution of these dopants is crucial to model their transport properties for further development of domain-wall electronic devices.⁵⁷

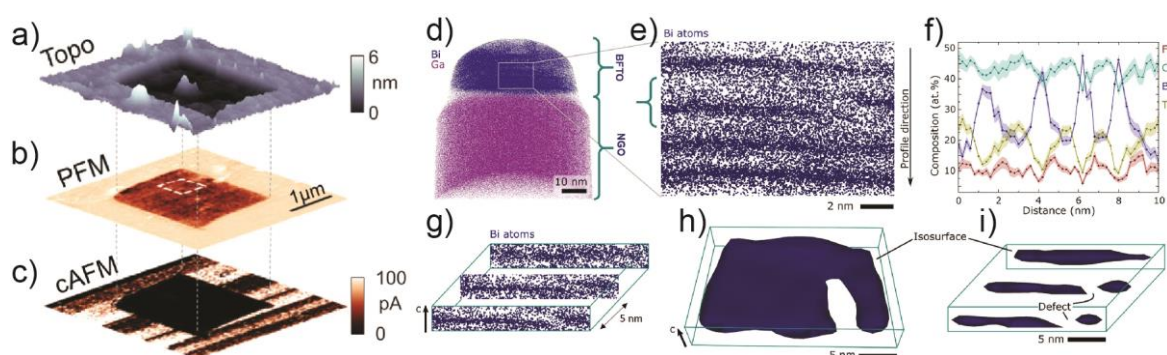


Figure 4: Invasive three-dimensional characterization of ferroelectrics. a) - c) topography a), piezoresponse force microscopy image showing domain structure b), and local conductivity obtained with conducting atomic force microscopy c) of a BaTiO_3 film after removal of the capping SrRuO_3 layer. a) - c) Reproduced with permission from ⁴⁰, copyright (2019) by the American Physical Society. d) Three-dimensional tomographic reconstruction of a needle of $\text{Bi}_5\text{FeTi}_3\text{O}_{15}$ prepared for atom probe tomography. e) Reconstruction of the Bi content in the central part of the needle. f) Profile of the Fe, Bi, Ti and O profile along the thickness of the $\text{Bi}_5\text{FeTi}_3\text{O}_{15}$ film. g) Reconstruction of a structural defect through the volume of the film. h), i) Isosurfaces around an out-of-phase boundary in the $\text{Bi}_5\text{FeTi}_3\text{O}_{15}$ film containing a high Bi density. d) - i) Reproduced with permission from ⁵⁶, copyright 2022 by the American Chemical Society.

3.2. Non-invasive and operando ferroelectric characterization using optical second-harmonic generation

The long probing depth of optical and X-ray based techniques has been instrumental for the characterization of materials, especially when they are buried under an

electrode or in a more complex device architecture⁵⁸ Here, we will focus on optical SHG which offers efficient and direct access to the polarization of ferroelectric materials. Excellent reviews^{59,60} have previously described the principle of the optical SHG process. Thus, we will only provide a brief description of the technique here. Optical SHG denotes the frequency-doubling of light in a non-centrosymmetric material. Because all ferroelectric materials break inversion symmetry by definition, SHG has emerged as a powerful tool to investigate these functional materials.^{61–66} In the electric-dipole approximation, information about the symmetry of the material, as well as the direction and magnitude of the ferroelectric polarization can be retrieved via SHG investigations. The intensity I_{SHG} of the conversion process depends quadratically on the induced second-order polarization $\mathbf{P}(2\omega)$ and therefore on the fluence of the incident laser, which is described by the electric field strength $\mathbf{E}(\omega)$ of the incident light:

$$I_{\text{SHG}} = |\mathbf{P}(2\omega)|^2, \quad \text{with } \mathbf{P}(2\omega) \propto \chi^{(2)} \mathbf{E}(\omega)\mathbf{E}(\omega).$$

Commonly, ultrashort light pulses are used to obtain a very high density of photons. This further opens the opportunity to study the temporal evolution of the polarization. The tensor elements of the non-linear electrical susceptibility $\chi^{(2)}$, which are defined by the point group symmetry and the spontaneous polarization of the material under investigation governs the angular dependence of the SHG light emission. All the components of the second-order susceptibility tensor can be accessed individually by performing SHG polarimetry experiments. Here, the incoming light pulse is linearly polarized, and the direction of the polarization is adjusted using a half-wave plate. The polarization of the emitted frequency-doubled light is selected with a Glan-Taylor prism prior to detection. A sketch of a conventional experimental setup for SHG is depicted in Figure 5a. In a SHG experiment, all $\chi^{(2)}$ -components with a parallel component to the propagation axis of the light wave are inaccessible. Hence, a careful selection of the angle of incidence of the fundamental beam allows for selective sensitivity to in-plane or out-of-plane polarization orientations. In addition to the typical integrated measurements obtained with the use of a photomultiplier tube, the insertion of a microscope objective and a camera further allows for spatially resolved measurements. This mode is particularly interesting when the domain structure of a ferroelectric material is of interest.

Limitations of optical SHG and comparison with other techniques – Despite the advantages mentioned above, optical SHG exhibits limitations in comparison to other methods. Other reviews have detailed the benefits and drawbacks of SHG compared to other ferroelectric characterization methods to a large extent already^{44,66}. We will, thus, provide only a brief overview over the most relevant techniques for investigating ferroelectric materials. Table 1 addresses the most important features of optical SHG, PFM, STEM, and electrical characterization methods to study the polarization of ferroelectrics embedded in a device heterostructure. In comparison with PFM and STEM, which provide nanoscale and atomic resolution, respectively, optical SHG microscopy is constrained by the optical resolution limit. By applying near-field techniques, the spatial resolution can be improved to reach about 10 nm.⁶⁷ We highlight that optical SHG is, similarly to integrated electrical measurements, more suitable for experiments when the net macroscopic polarization is of interest.

Operando studies of polarization dynamics during electric-field application have been performed with optical SHG, STEM, scanning electron microscopy (SEM), and electrical characterization methods.^{23,68,69} STEM measurements, however, require the fabrication of a lamella and therefore fall into the category of destructive techniques. With optical SHG and PFM, the polarization magnitude cannot be quantitatively determined, but the direction and relative amplitude can be retrieved in three dimensions. STEM and electrical characterization methods, on the contrary, provide the polarization magnitude and direction, yet within a projected plane orthogonal to the zone axis and along the direction of the electric field, which is defined by the capacitor geometry, respectively. For studying the temporal evolution of the polarization, optical SHG and electrical characterization methods are superior to PFM and STEM as they allow for a faster acquisition rate and higher temporal resolution. Finally, optical SHG, PFM and electrical characterization methods are tabletop experiments that can be readily performed. Optical SHG can even be integrated into deposition systems for in-situ analysis during the insertion of the ferroelectric material into a multilayer stacking.

Hence, from these brief considerations, we conclude that only the combination of different techniques can lead to a complete understanding of the ferroelectric properties in device architectures. Nanoscale investigations, for example, require both PFM and STEM analysis. If the macroscopic polarization or the fast electric-field-induced switching dynamics are of interest, the combination of optical SHG and electrical characterization methods will be superior.

Table 1: Overview over the advantages and drawbacks of common characterization methods for ferroelectrics embedded in a device heterostructure.

	SHG	PFM	STEM	Electrical characterization
Spatial resolution	~ μm	~nm	~pm	Integrated measurement
Examined area	μm -mm	μm	nm	nm-mm
Destructive	No	No	Yes	No
Polarization mapping	3D	3D	2D	1D
Quantitative evaluation of P	No	No	Yes	Yes
Temporal resolution	<ps	~50 μs ²²	~100 ms ⁷⁰	ns
Tabletop	Yes	Yes	No	Yes

In the following, we will highlight how optical SHG supports the integration of ferroelectrics into energy-efficient oxide electronics. We describe the most recent findings obtained through operando investigations of ferroelectric capacitors, non-invasive characterizations of ferroelectric domain walls, and in-situ probing of polarization states during the epitaxial growth.

Operando investigation on ferroelectric capacitors – The seminal demonstration of the highly desired electric-field-induced magnetization reversal using a multiferroic magnetoelectric material²² triggered intense research effort towards the search for

multiferroic material systems^{5,71–74} and the energy-efficient manipulation of magnetic states using voltage only.⁷⁵ The room-temperature electric-field control of the ferromagnetic order was realized in a BiFeO₃/Co₉₀Fe₁₀ bilayer.²² The net magnetization reversal in absence of an external magnetic field in the Co₉₀Fe₁₀ layer is based on the one-to-one domain matching between the multiferroic domains in BiFeO₃ and the ferromagnetic domains in the top Co₉₀Fe₁₀ layer, such that a reversal of the net polarization in the magnetoelectric compound would result in the net reversal of the magnetization in the exchange-coupled Co₉₀Fe₁₀ layer. The switching mechanism, and the corresponding domain correlation, was determined by destructive analysis and the removal of the Co₉₀Fe₁₀ active element.⁷⁶ Following investigations involving a scanning-electron-microscopy-based approach confirmed the domain correlation in the pristine state.⁷⁷ Non-invasive SHG experiments on BiFeO₃/Co₉₀Fe₁₀-based capacitors combined with magnetometry further allowed to track the coupled directions of the net polarization of the multiferroic layer and of the magnetization in the Co₉₀Fe₁₀ after electric-field application to the capacitor.⁴⁸ Such a direct access to the ferroelectric domains of magnetoelectric materials after electric-field application is key to the understanding and further development of magnetoelectric-based devices. Here, the local in-plane polarization reorientation, depicted in Figures 5b–5d, was correlated to the magnetic domain reorientation in the top magnetic electrode, revealing the persistence of the one-to-one matching of the multiferroic and ferromagnetic domains in the MESO device architecture. This demonstration was soon followed by more device-relevant experiments with chemically substituted films and smaller active capacitor sizes.²³ The substitution of 15% of the Bi cations by La reduces the coercive field, i.e. the amplitude of the voltage pulses to switch the net polarization of the multiferroic constituent, a vital aspect to perform in-memory logic using La_{1-x}Bi_xFeO₃ in MESO devices. It comes, however, at the expense of a disordered domain structure and hence a possible loss of the functionality since a net macroscopic polarization is needed to deterministically drive the net magnetization of the ferromagnetic layer in the MESO structure. SHG investigations revealed that a weak net polarization persists in the La_{0.15}Bi_{0.85}FeO₃ thin-films. Strikingly, the operando characterization during electrical cycling of the devices showed that the net polarization in the multiferroic layer can be strongly enhanced, see Figures 5e and 5f. Beyond the capacity to access ferroelectric states in device architectures the SHG process is compatible with time-resolved experiments and hence may be instrumental in the determination of energy-efficient device operation and magnetoelectric switching events.

Ferroelectric domain wall architecture – The internal structure of domain walls is crucial for the development of the devices presented in section 2. The emergence of the NC effect in multi-domain ferroelectric/dielectric heterostructures²⁸ as well as the memristive behaviors of FeFETs²⁶, FTJs³⁴ or domain-wall-conduction-based RAMs³⁸ root in the existence and internal properties of ferroelectric domain walls. In thin films of the model system PbZr_{0.2}Ti_{0.8}O₃, optical SHG has been instrumental in the demonstration of the Néel-type character of 180° ferroelectric domain walls.^{37,78} Because the optical configuration of the SHG approach establishes selectivity over the $\chi^{(2)}$ -components, as described above, a normal-incidence optical configuration allows to detect solely in-plane polarized components, and hence, a Néel contribution of a domain wall within an out-of-plane polarized PbZr_{0.2}Ti_{0.8}O₃ matrix, see Figures 5g–5i.

SHG polarimetry at the walls indicated a polarization projection perpendicular to the domain wall, ruling out a Bloch-type polarization of the walls. Further studies on LiTaO₃ revealed Néel- and Bloch-type ferroelectric walls using SHG.⁷⁸ Such studies highlight striking analogies between ferroelectric and ferromagnetic orders. In light of the recent studies describing an electric analogue of the notorious Dzyaloshinskii-Moriya interaction (DMI) in magnetically ordered systems⁷⁹, the ability to track the internal structure of ferroelectric domain walls is essential for the development of chiral polar textures. Once again, the combination of the non-invasive nature of SHG and its compatibility with time-resolved investigations enables the determination of the dynamics of polar textures under various excitations.

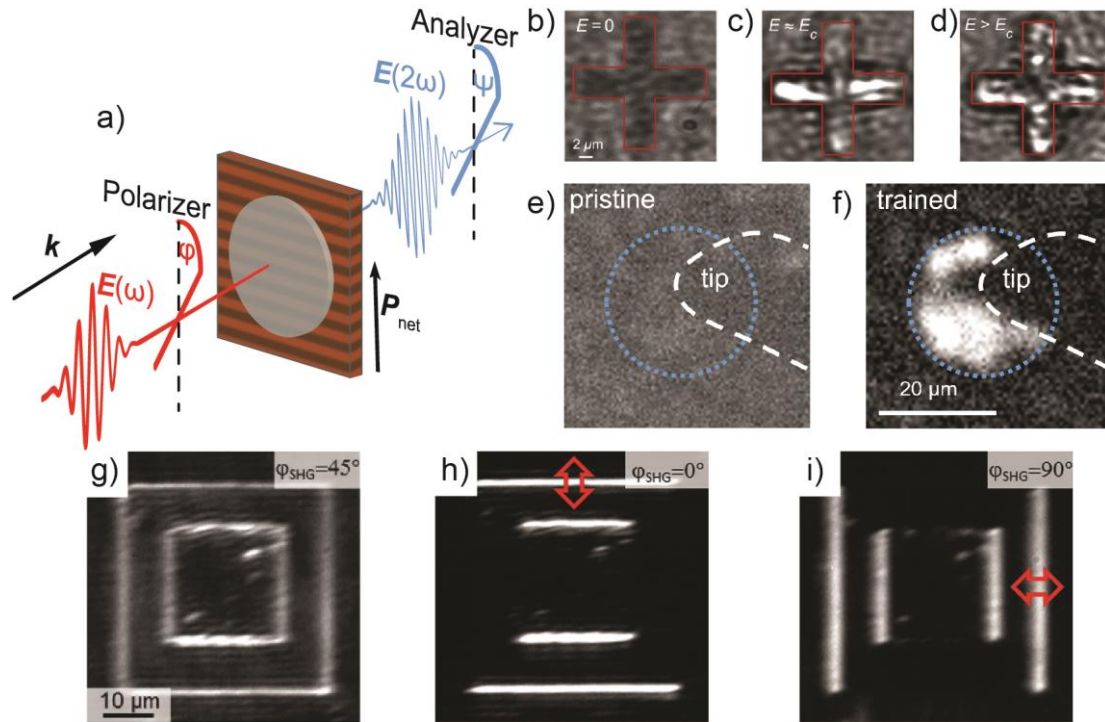


Figure 5: Optical second-harmonic generation as a versatile tool to probe ferroelectric properties of devices. a) Schematic sketch of an optical second-harmonic generation experiment. The polarizer is a half-wave plate that rotates the linearly polarized laser beam by an angle φ . The analyzer is a Glan-Taylor prism which rotates the polarization of the frequency-doubled light by the angle Ψ . b)–d) The direction of the net in-plane polarization of a BiFeO₃ film underneath a cross-shaped electrode was spatially resolved using optical second-harmonic generation in b) the pristine case, and after voltage application c) close to the coercive field and d) beyond the coercive field. The bright regions depict a rotation of the net in-plane polarization away from the pristine axis. Reproduced with permission from ⁴⁸, copyright (2018) by the American Physical Society. e), f) Operando second-harmonic generation study on circularly shaped La_{0.15}Bi_{0.85}FeO₃/Co₉₀Fe₁₀ devices showing e) an almost entirely suppressed net in-plane polarization in the pristine state and f) a strong net in-plane polarization after electric field training. Reproduced with permission from ²³, copyright (2021) by Wiley-VCH. g)–i) Optical second-harmonic generation identifies the Néel character of ferroelectric domain walls in PbZr_{0.2}Ti_{0.8}O₃. Reproduced with permission from ³⁷, copyright (2017) by Wiley-VCH.

Polarization tracking during thin-film deposition – As described above, non-invasive SHG investigations have been carried out operando on device architectures. On top of that, SHG has been also used to monitor the ferroic properties directly during the thin-film deposition process by introducing a SHG probe beam into the physical vapor deposition chamber. The first investigations using this approach have been performed on magnetic metals in the late 90s.^{80,81} There, tracking the SHG signal

during the growth of Co and Ni films allowed the detection of the onset of magnetism, as well as the temperature-dependent reorientation of the magnetic anisotropy. This technique was further used to determine the exchange-coupling strength of antiferromagnetically coupled layers. In-situ monitoring of oxide thin-film growth using SHG was only mentioned years later in the proof-of-concept study by Rubano *et al.*⁸². The first implementation of a SHG probe in an oxide pulsed laser deposition chamber has been reported in 2017.⁹ A schematic representation of the experimental setup within the growth chamber is depicted in Figure 6a. In their study, De Luca *et al.* performed an in-situ SHG (ISHG) investigation during the growth of thin films of the model ferroelectric BaTiO₃ and multiferroic BiFeO₃ and demonstrated the ability to track ferroelectricity during the epitaxial deposition process.⁹ Because ISHG can be used in combination with other in-situ growth monitoring tools, such as reflection high-energy electron diffraction (RHEED), which provide information on the growth modes and growth rate, the critical thickness for the emergence of ferroelectricity in BaTiO₃ and BiFeO₃ could be quantified with unit-cell accuracy.⁹ Hence, the invention of ISHG as a novel characterization tool for epitaxial oxide thin-film growth opened a whole new world of investigations. Because of the strong impact of the epitaxial strain on the ferroelectric transition temperature, most ferroelectric materials grow in the ferroelectric phase during the physical deposition process even at elevated deposition temperatures of 700 °C.¹⁴ ISHG is emerging as a key technique to understand the influence of the processing steps on the final polarization states in technology-relevant systems. In addition to the direct access to the strain-, thickness-, and temperature-dependent polarization, ISHG can also reveal important information on ferroelectric domain formation during growth. Any deviation from an out-of-plane-oriented single-domain state translates into a reduction of the total ISHG yield. Figure 6 provides a summary of the information that became accessible through the ISHG approach. In tetragonal ferroelectrics such as BaTiO₃, Pb[Zr_{1-x}Ti_x]O₃ and PbTiO₃, the domains can be in-plane or out-of-plane polarized, depending on the epitaxial strain and film thickness. By tracking the ISHG signal in a configuration that is sensitive to the out-of-plane-oriented domains, the real-time observation of strain-dependent domain conversion has been reported during the growth.⁸³ Beyond a simple polarization reorientation, SHG can further monitor the formation of a complex domain architecture during the growth. Oppositely oriented domains emit SHG waves with a phase shift of 180°.⁵⁹ Hence, the formation of a high density of 180° domain walls results in destructively interfering SHG waves and a net suppression of the ISHG signal. Thus, ISHG provides unique insights into polarization suppression mechanisms in thin films towards an improved understanding of the physics of ferroelectricity in the ultrathin regime.

Most importantly, real time ISHG monitoring was proven irreplaceable to track transient phenomena during ferroelectric thin film growth. In the next section we will detail how the evolving electrostatics during and after growth, as well as surface and interface-related effects are now being engineered to control and enhance the polarization of thin films.

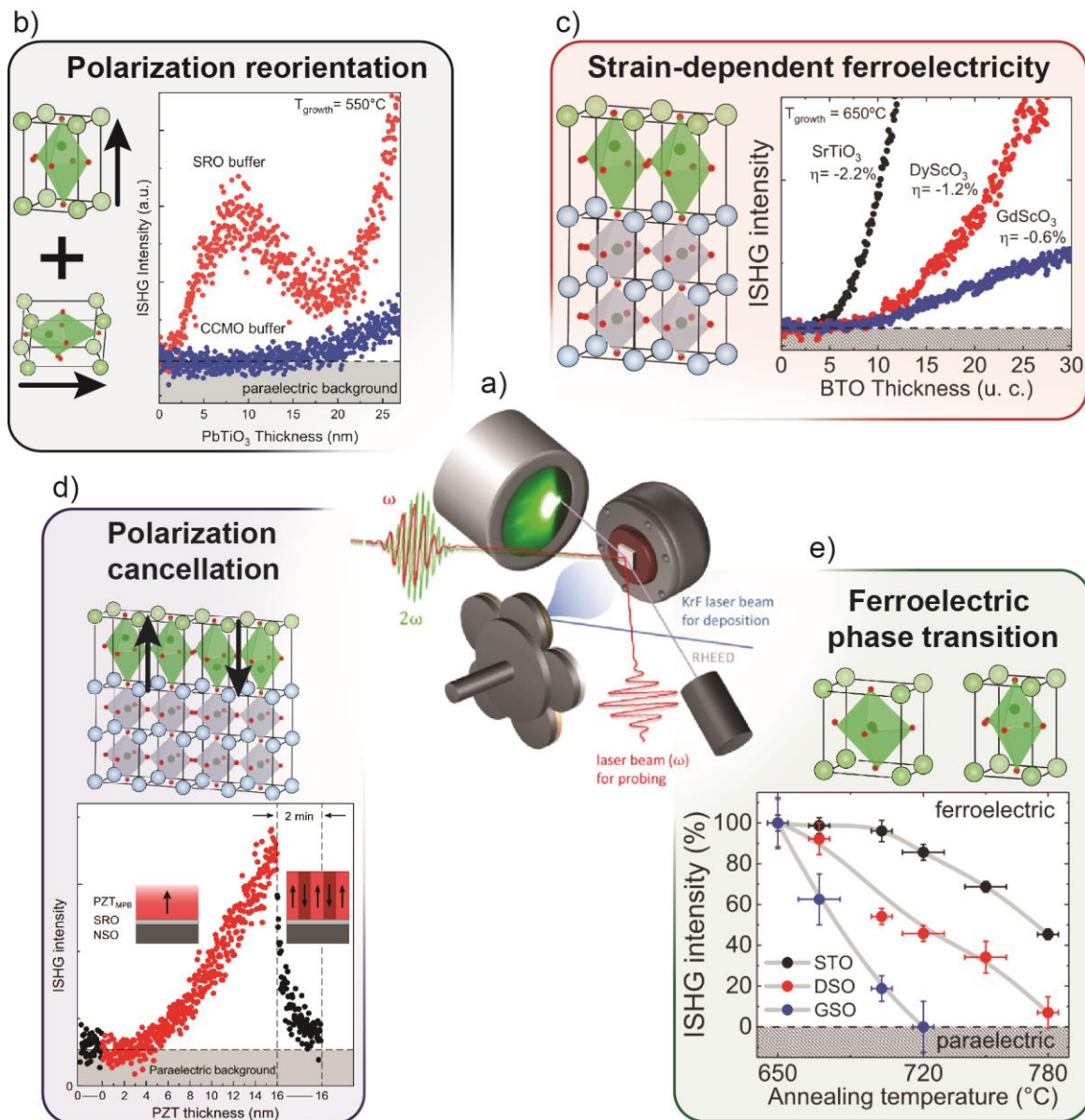


Figure 6: The power of in-situ second-harmonic generation investigations for the design of polarization in the ultrathin regime. Reproduced with permission from ⁹, copyright (2017) by the Nature Publishing Group. a) Schematic representation of the in-situ second-harmonic generation setup alongside a reflection high-energy electron diffraction setup in the pulsed laser deposition chamber. b) In-situ second-harmonic generation showing the partial conversion from out-of-plane-oriented c-domains into in-plane-oriented a-domains after a few nanometers (red data points) or from the first deposited unit cell (blue data points) during the growth of PbTiO_3 on SrRuO_3 and $\text{Ce}_{0.04}\text{Ca}_{0.96}\text{MnO}_3$ buffers, respectively. Reproduced from ⁸³, copyright (2020) with the permission of AIP Publishing. c) In-situ second-harmonic generation signal depicting the strain-dependent polarization enhancement during the growth of BaTiO_3 . Reproduced with permission from ⁴⁰, copyright (2019) by the American Physical Society. d) In-situ second-harmonic generation signal tracking the net polarization emergence and cancellation of $\text{PbZr}_{0.52}\text{Ti}_{0.48}\text{O}_3$ during and after the growth, respectively. The insets depict the domain structure during and after the growth. Reproduced with permission from ⁸⁴, copyright (2022) by the Nature Publishing Group. e) In-situ second-harmonic generation depicting the strain-dependent ferroelectric phase transition of BaTiO_3 . Reproduced with permission from ⁴⁰, copyright (2019) by the American Physical Society.

4. TOWARDS ROBUST AND DETERMINISTIC FERROELECTRIC BEHAVIOR IN THE ULTRATHIN REGIME

4.1 Enforcing polar displacements at interfaces

Pushed by the need for miniaturization, the demand for low-voltage operation, and boosted by the development of FTJs, intense efforts are devoted to the stabilization of a robust ferroelectric behavior in layers of only a few unit cells in thickness. Hence, finding strategies to combat the detrimental impact of the depolarizing field, which suppresses the polarization in the ultrathin regime has been a long-standing challenge. Non-centrosymmetric metals, so-called polar metals, once inserted as conducting buffer layers in ferroelectric capacitors, have been predicted to suppress the critical thickness for ferroelectricity in the ferroelectric layers.⁸⁵ The inversion-symmetry-lifting displacements present in the polar metal buffer, such as LiOsO_3 , can enforce the onset of a polarization in an adjacent ferroelectric material such as BaTiO_3 and lead to a vanishing critical thickness in nanoscale capacitors.⁸⁵ Such non-centrosymmetric metals are, however, very scarce and the experimental characterization of polar states in a conducting matrix have remained challenging. Furthermore, the existing systems are structurally incompatible with most of the technologically relevant perovskite ferroelectrics, making their implementation in heterostructures unfeasible. Thus, epitaxial strain has remained the most promising approach to enforce ferroelectric distortions in ultrathin layers. In BiFeO_3 thin-films, a sizeable (>4%) epitaxial compressive strain⁸⁶ was shown to stabilize a super-tetragonal phase at elevated growth temperatures.^{87–89} The significant unit-cell distortion coupled with the increased energy for domain-wall formation was reported to induce polarization from the very first unit cell⁸⁷. The vast majority of ferroelectrics, however, cannot accommodate such a high epitaxial strain and relax by creating detrimental misfit dislocations, rendering this approach inapplicable. Hence, additional routes towards the stabilization of ultrathin ferroelectricity remain to be established.

4.2. Polarization enhancement using cooperative surface contributions

Progress in the epitaxial design of electrically ordered thin-films at the atomic level led to the discovery of interface-induced antiferroelectric ordering, as well as exotic polar and antipolar phases in various materials.² The electrostatic boundary conditions of thin films are routinely engineered to stabilize a polar phase or establish a preferred polarization direction in thin-film heterostructures.⁹⁰ In particular, the control of the buffer surface termination has emerged as a key ingredient for the design of interfaces with preferential charge screening properties. By preselecting the AO or BO_2 planes, which can exhibit different charge states in the ABO_3 perovskites system, one can deterministically induce the growth of ferroelectric layers with upwards- or downwards-oriented polarization.⁹ The polarization of ultrathin films can also be influenced by tuning the electrostatic boundary conditions at the top surface through adsorbates or charge screening via the growth atmosphere.^{91,92}

Hence, by engineering top and bottom surface contributions to support the onset of a common polarization direction, the enhancement of the polarization of the thin film can be envisioned. Monitoring the polarization during growth allows the identification of the

distinct contribution from each surface. Only recently, ISHG experiments allowed to disentangle the contributions from the top and bottom surface to the final polarization state of PbTiO_3 thin-films and provided real-time experimental access to transient polarization states during the epitaxial deposition, see Figures 7a. While the bottom interface is well defined by the crystal structure of the buffer and its electrostatic screening, the top surface consists of a growth front where deposition material is continuously supplied. The ISHG analysis revealed that during growth, the polarization is solely driven by the bottom interface. Once the growth is interrupted, the top surface consolidates and suddenly contributes to the final polarization state of the film. For A-site-volatile materials, such as Pb- or Bi-containing ferroelectrics, a surface off-stoichiometry emerges and leads to Pb- or Bi-rich, charged surface layers, which can eventually screen the bound charges and thus contribute to an enhancement of the polarization.⁹²

This ISHG study revealed the important role of such surface off-stoichiometries and the formation of a positively charged surface reconstruction during the deposition of A-site volatile ferroelectric materials in favoring a downwards-oriented polarization.^{90,92}

Finally, by selecting a buffer termination favoring the polarization state, which is also stabilized by the top surface, an interface synergy effect was observed and a robust ferroelectric behavior in films of only a few unit cells in thickness was demonstrated, even when capped with a non-screening dielectric SrTiO_3 layer, see Figure 7b. This work highlighted the importance of cooperative interface contributions towards the stabilization of robust ferroelectric behavior as a key ingredient for the successful integration of ferroelectric films into nanoscale device architectures.⁹²

4.3. In-situ monitoring of domain formation for memristive-type applications

As described in section 2.4, the controlled generation of oppositely oriented domains and the concurrent tunability of the net polarization can be conveniently exploited to realize a change in electroresistance in FTJ devices. Since the pioneering demonstration of a ferroelectric memristor device⁹³ using electrical pulses to generate quasi-infinite resistance states in a ferroelectric capacitor, efforts have been devoted to controlling the polarization in ultrathin films. Typically, strategies to optimize the domain structure and switching mechanisms rely on strain tuning and chemical doping approaches. For instance, choosing the extent of epitaxial compressive strain in tetragonal ferroelectric materials allows balancing the mixture of out-of-plane and in-plane-oriented domains. In addition, controlling the B-site occupancy in the $\text{Pb}[\text{Zr}_{1-x}\text{Ti}_x]\text{O}_3$ family can trigger a structural competition at the so-called morphotropic phase boundary (MPB), where the flattened energy landscape can give rise to domain configurations with unconventional switching pathways and high susceptibility to the electric-field.⁸⁴ Surprisingly little efforts have been devoted to studying the combined effect in strain-engineered MPB thin-films and only a few reports deal with MPB ferroelectric epitaxial thin-films.^{84,94}

Using ISHG, the investigation of the polarization of $\text{PbZr}_{0.52}\text{Ti}_{0.48}\text{O}_3$ films at the morphotropic composition during the growth on various substrates revealed the capacity to design films with unprecedented ferroelectric switching behavior.⁸⁴ The direct access to the polarization during epitaxial design allowed finding the balance of increased electric-field susceptibility in the vicinity of the MPB and anisotropic

compressive epitaxial strain to stabilize the formation of nanometric domains in the films. The anisotropic epitaxial strain induces lateral strain distributions in the films that translate into a distribution of coercive fields in the ferroelectric layer. Using a scanning probe tip, the local application of the electric field allows to locally tune this nanometric domain population and hence to reach any net polarization state from saturation to complete depolarization, simply by applying a DC bias, see Figures 7c and 7d. A proof-of-concept experiment involving C-AFM revealed that the locally created quasi-continuous net polarization levels indeed correspond to distinct resistance states, see Figure 7e.⁸⁴ Because of the nanometric dimensions of the domains, such an achievement enables further reduction of the lateral dimensions of ferroelectric memristors.

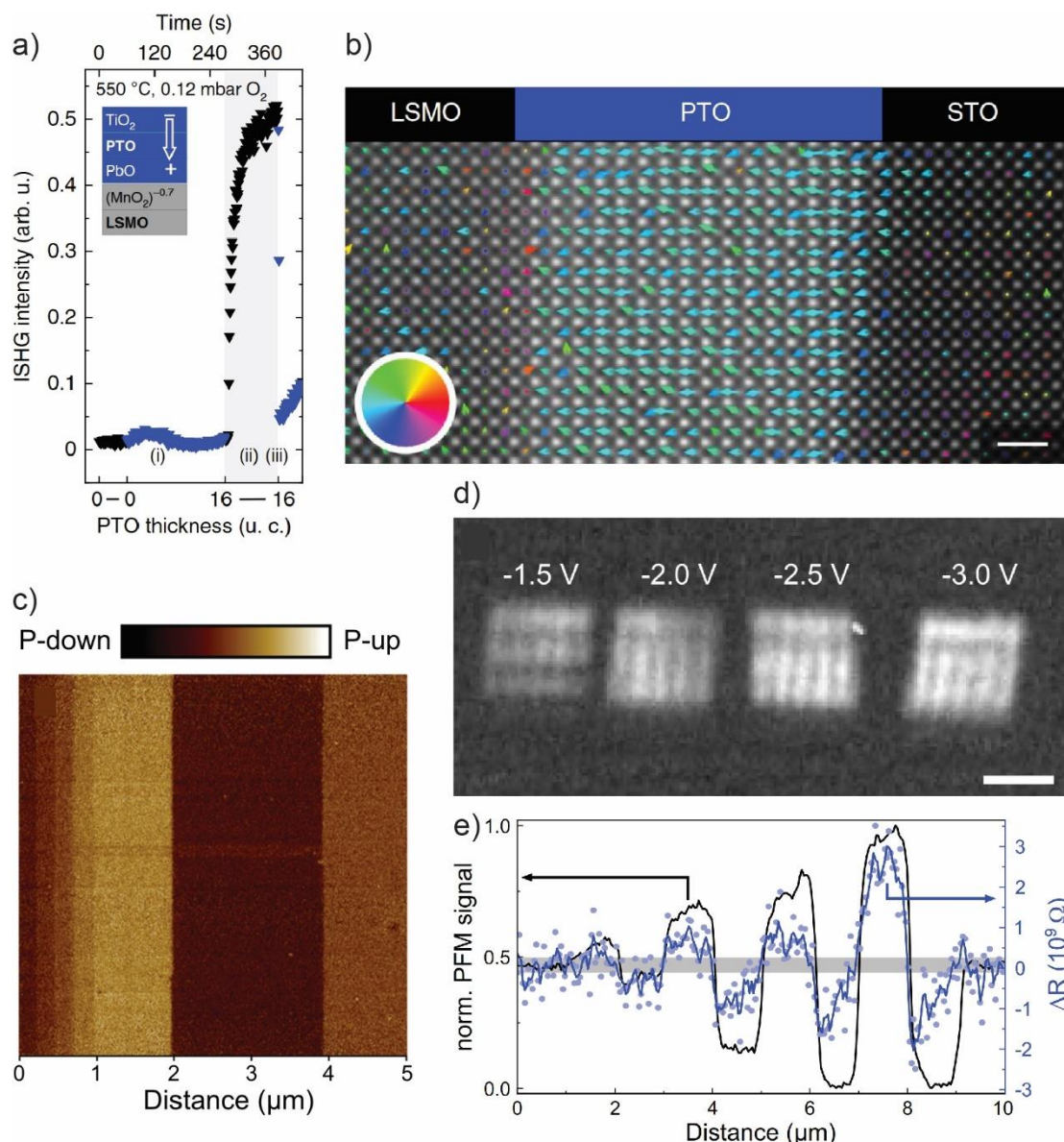


Figure 7: Deterministic control over the net out-of-plane polarization magnitude. a) In-situ second-harmonic generation signal depicting the polarization enhancement from cooperative interfaces after the growth of PbTiO_3 was halted (black filled symbols). The inset depicts the cooperative electrostatics from the interfacial planes. b) Scanning transmission electron microscopy map of the dipole moments after the growth of a $\text{SrTiO}_3/\text{PbTiO}_3/\text{La}_{0.7}\text{Sr}_{0.3}\text{MnO}_3$ heterostructure. The direction of the dipole moment is depicted with the color of the arrow (see the color wheel) and the magnitude of the dipole moment is depicted with the length of the arrow. a) and b) Reproduced with permission from ⁹², copyright (2020)

by the Nature Publishing Group. c) Vertical-piezoresponse force microscopy image of the polarization magnitude after incrementally reverse poling a $\text{PbZr}_{0.52}\text{Ti}_{0.58}\text{O}_3$ thin film. d) Second-harmonic generation image depicting the gradual increase in net polarization magnitude for four squares that were poled with gradually increasing voltage. e) Modulation of the ohmic resistance (blue curve) with different net polarization states depicted by the piezoresponse force microscopy signal (black curve). c)–e) Reproduced with permission from ⁸⁴, copyright (2022) by the Nature Publishing Group.

4.4. Overcoming the limitations imposed by the depolarizing field using in-plane polarized films

Another approach in defeating the depolarizing field effects relies on working with ultrathin ferroelectric films that are polarized within the plane of the film. Unlike out-of-plane ferroelectrics that possess a critical thickness of a few unit cells⁹, in-plane-polarized films are expected to be less affected by the depolarizing field, since the bound-charge accumulation is now taking place within the lateral dimension of the film.⁸³ In-plane polarization emerges spontaneously in layered ferroelectrics. The Aurivillius compounds⁹⁵ of general formula $\text{Bi}_2\text{A}_{n-1}\text{B}_n\text{O}_{3n+3}$, characterized by unit cells that consist of perovskite planes interleaved by fluorite-like Bi_2O_2 planes, stand out by virtue of their excellent ferroelectric switching properties⁹⁶ and potential for hosting multiferroicity⁹⁷. The thin-film growth of single crystalline films has been reported using atomic vapor deposition⁹⁸ and pulsed laser deposition⁹⁹. Nevertheless, the layer-by-layer growth mode of these structures, enabling their thickness control with sub-unit-cell precision, was only demonstrated recently, see Figures 8a–8c and 8h.^{100,101} It confirmed that 0.5-unit-cell-thick Aurivillius films are ferroelectric and exhibit an in-plane-polarized stripe domain configuration.¹⁰⁰ In agreement with this, sub-unit-cell ferroelectricity was also shown in exfoliated 2D Aurivillius flakes.¹⁰² These measurements confirmed the robustness of in-polarized layered materials against the detrimental effects of the depolarizing field. The achievement of high quality, twin-free films enabled the investigation of domain engineering in the Aurivillius materials. The first studies indicated the ability to control the formation of structural defects in the layered structure of the films using substrate morphology, see Figures 8d–8g.⁵⁶ The ordering of the so-called steric out-of-phase boundaries, appears as key in the controlled formation of in-plane polarized ferroelectric domains.

Furthermore, the structural compatibility of the Aurivillius compounds with the established perovskite systems enables the epitaxial growth of heterostructures combining both in-plane and out-of-plane independent polar anisotropies. This has remained elusive in perovskite-based multilayers as the epitaxial strain in oxide heterostructures most commonly supports the emergence of a uniform polarization in every constituent layer. Heterostructures consisting of an in-plane-polarized Aurivillius buffer and an out-of-plane-polarized perovskite film, in contrast, allow the design of interfaces with orthogonal polarization states, emulating polarization configurations of neutral ferroelectric domain walls or a flux-closure domain pattern. The resulting polarization continuity and partial flux closing at the interface minimize depolarizing-field effects and, thus, stabilize the out-of-plane polarization from the very first unit cell in the classical ferroelectrics BaTiO_3 and BiFeO_3 .¹⁰³

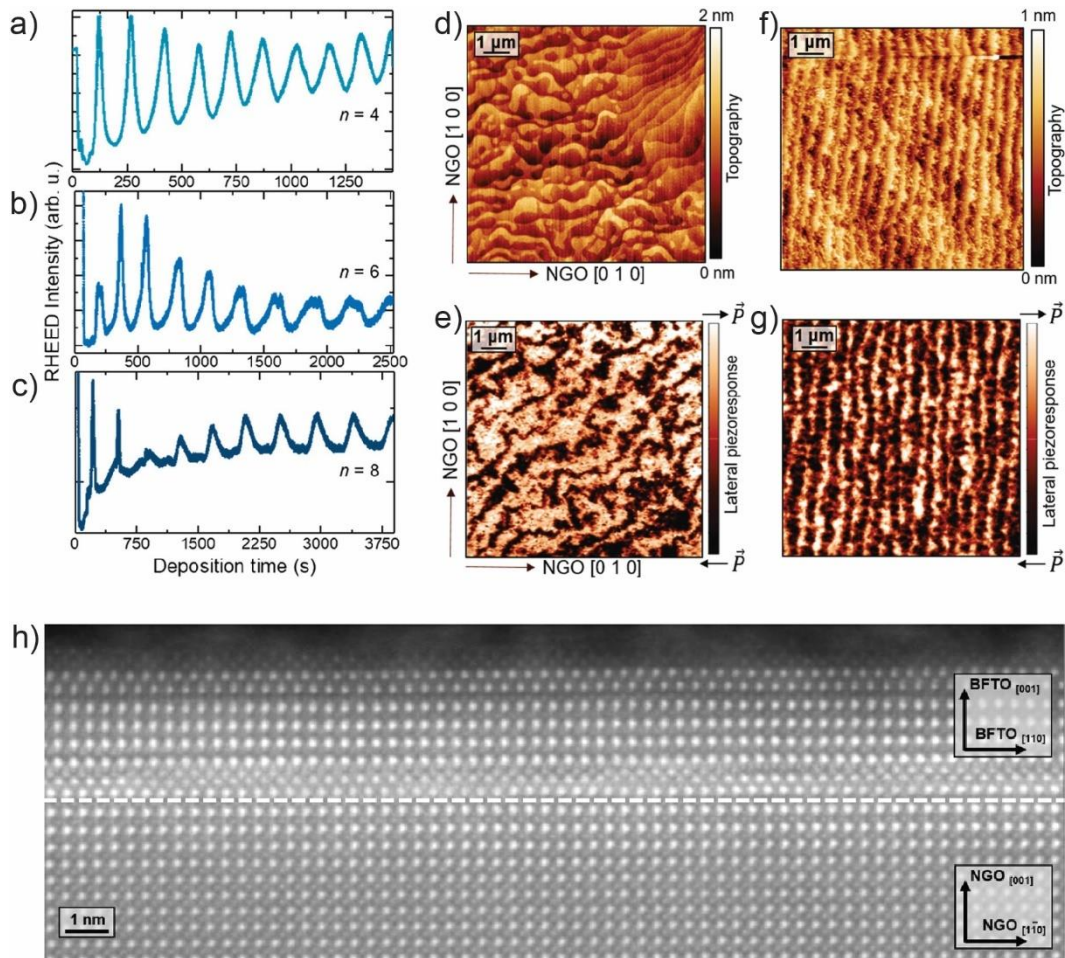


Figure 8: Control over the growth and domain formation of ultrathin Aurivillius films. a)–c) Reflection high energy electron diffraction intensity oscillations demonstrating the layer-by-layer growth of $\text{Bi}_{n+1}\text{Fe}_{n-3}\text{Ti}_3\text{O}_{3n+3}$ films with $n = 4, 6$ and 8 with half unit-cell precision. a)–c) Reproduced with permission from ¹⁰¹, copyright 2021 by the American Chemical Society. d)–g) The topography of the NdGaO_3 (001) substrate, depicted in d) and f) determines the formation of ferroelectric domains, as depicted in the corresponding lateral-piezoresponse force microscopy images e) and g). d)–g) Reproduced with permission from ⁵⁶, copyright 2022 by the American Chemical Society. h) High-resolution high-angle annular dark-field scanning transmission electron microscopy image demonstrating that a half unit-cell coverage of $\text{Bi}_5\text{FeTi}_3\text{O}_{15}$ can be achieved during the growth. Reproduced with permission from ¹⁰⁰, copyright (2020) by Wiley-VCH.

5. EMERGING CONCEPTS IN ELECTRICALLY ORDERED SYSTEMS

As we have mentioned before, it is challenging to maintain a robust out-of-plane-oriented polarization, while the thickness of ferroelectrics shrinks. This is predominantly because of the pronounced impact of the depolarizing field and interface contributions at reduced dimensions. In this final section, we will cover emerging research directions, which offer promising approaches for the establishment of ferroelectric behavior in the ultrathin regime.

5.1. Two-dimensional ferroelectrics

Layered van der Waals (vdW) materials that feature strong intralayer and weak interlayer bonding allow for the convenient fabrication of atomically thin 2D sheets via exfoliation and have recently emerged as a promising materials family for the design

of 2D ferroelectrics^{104,105}. In contrast to the previously discussed family of layered Aurivillius materials, out-of-plane polarization may emerge in vdW ferroelectrics. The absence of dangling bonds, the insensitivity to boundary conditions, and the compatibility with any substrate material – even in the monolayer limit – offers large potential to engineer miniaturized ferroelectric devices using 2D vdW ferroelectrics.

Despite their immense application potential, to date, only a handful of vdW materials have been discovered that are intrinsically ferroelectric down to the monolayer limit. Amongst them, some monolayers exhibit a fully in-plane-oriented polarization¹⁰⁶ and only a few selected compounds, including MoTe₂¹⁰⁷, In₂Se₃¹⁰⁸, and CuInP₂S₆¹⁰⁹ feature the sought-after out-of-plane polarization. In addition to their scarcity, the remanent polarization of intrinsic vdW ferroelectrics is often relatively small (<1 $\mu\text{C}/\text{cm}^2$) and the material selection is restricted to compounds with a polar space group of their bulk counterpart.

In a series of studies^{105,110,111}, it was recently shown that the previous limitation to polar vdW materials and hence, to obtain ferroelectricity in 2D materials can be overcome by artificially stacking non-polar vdW sheets into metastable non-centrosymmetric assemblies. Here, in analogy to the exciting physics around the twist angle in graphene-based multilayers, the relative arrangements of stacked 2D materials can trigger an out-of-plane polarization. The spontaneous polarization in these artificial 2D ferroelectrics is switchable via an applied electric field and the reversal of the out-of-plane polarization occurs via the lateral sliding of one layer on top of the other, coining the term “sliding ferroelectricity”^{104,112} for this switching mechanism. Figure 9a depicts this phenomenon for the case of a h-BN bilayer system. This opens the door for the creation of novel 2D ferroelectrics made from well-established centrosymmetric 2D materials, such as graphene¹¹⁰, transition-metal dichalcogenides¹¹³, and MXenes¹¹⁴.

The discovery of vdW ferroelectrics is a prime example that experimental techniques beyond the electrical approach, most importantly optical SHG, are necessary to observe and quantify a ferroelectric polarization in exotic and ultrathin materials.

5.2. Hafnia-based ferroelectrics

Before the first report on its ferroelectric behavior in 2011 by Böscke *et al.*¹¹⁵ amorphous HfO₂ had already been widely appreciated and mass-produced as a high-permittivity insulator for the gate oxide stack in miniaturized FETs¹¹⁶. Thus, the surprising discovery of ferroelectricity in CMOS-compatible HfO₂ and derived compounds, like Hf_xZr_{1-x}O₂¹¹⁷ and ZrO₂¹¹⁸, has quickly led to intense research and industrial efforts being devoted to study and develop these materials¹¹⁹.

Unlike typical perovskite ferroelectrics, the switchable polarization of doped HfO₂ systems demonstrates an extraordinary persistence against thickness reduction, even when integrated directly into the silicon platform, see Figures 9b and 9c.¹²⁰ The origin of the ferroelectricity and the untypical scaling behavior is still under intense debate, however.¹²¹ Recent first-principles investigations highlighted a polarization-emergence mechanism involving two phase transitions.¹²² First, an antipolar phase transition is triggered by epitaxial tensile strain, then a strong polar-antipolar coupling leads to the onset of ferroelectricity. In this picture, hafnia thin films are improper ferroelectrics where the antipolar order is the driving order parameter. This may contribute to the

understanding of the robustness of HfO₂ systems against the depolarizing field-related effects.

Owing to their compatibility with existing CMOS processes, the integration of HfO₂ and Hf_xZr_{1-x}O₂ into non-volatile memory devices, including FeRAMs, FeFETs, NC-FETs and FTJs has quickly progressed over the last years, despite missing a clear picture of the ferroelectric origin. In particular, for FeFETs, the high coercive field of HfO₂ is an important advantage to maintain a large memory window, while simultaneously reducing the thickness of the ferroelectric gate layer¹²³. Also, in FTJs fabricated with a 1 nm Hf_xZr_{1-x}O₂ tunnel barrier on silicon, recently, a very high electroresistance in conjunction with reasonably high read-out currents were realized³⁰.

Further understanding of the ferroelectricity in this material system is therefore of utmost importance to maximize the performance of and eventually establish ferroelectric HfO₂-based electronics in the consumer markets. Strikingly, to date, although promising SHG yields have been measured in HfO₂-based heterostructures^{124–126}, there are no SHG polarimetry-based symmetry investigations to determine the SHG active tensor elements of the films, suggesting a non-conventional optical SHG activity or polarization mechanism.

5.3 The concept of layer polarization

The concept of layer polarization has been developed recently in perovskite materials and describes the emergence of a lattice polarization as the consequence of the stacking of charged planes with alternating polarity.¹²⁷ To illustrate this concept, let us consider a (001)-oriented ABO₃ perovskite crystal. The unit cell consists of alternating AO and BO₂ atomic planes. If both, A and B, cations carry an ionic charge of +3 and the anions carry an ionic charge of -2, then the planes have formal charges of +1 and -1, respectively. Hence, building a crystal or a film by stacking unit cells starting with the BO₂ layer and ending with the AO surface termination, will induce a positive charge accumulation at the top surface, while the bottom interface is negatively charged. This leads to the so-called layer polarization in the perovskite materials. Unlike the spontaneous polarization, the layer polarization is not switchable in external electric fields and is not solely restricted to ferroelectric crystals. Layer polarization can develop in centrosymmetric compounds, too.

While the concept of layer charges is trivial in bulk materials due to the self-compensating quasi-infinite number of layers, in thin films where the structure is truncated with a surface, layer polarization results in uncompensated surface charges and thus can significantly affect the spontaneous polarization. In ferroelectric films, the layer polarization and the spontaneous polarization coexist. The direction of spontaneous polarization will be oriented such that the surface-bound charges can be screened by the ionic charges at the top and bottom atomic planes. If both the ferroelectric film and its buffer layer exhibit a layer polarization, one can consider the net charge at the interface for predicting the direction of polarization in the film. Interestingly, in BiFeO₃, the layer polarization has been calculated to a value matching the ferroelectric polarization. This suggests the possibility to suppress the ferroelectric bound charge accumulation in specific orientation and termination states and suggest new avenues for catalytic activity at the surface and interesting ferroelectric behaviour at the nanoscale.¹²⁸

In a recent first-principles study, it has been shown that an uncompensated layer polarization can itself trigger a ferroelectric-like distortion. As depicted in Figures 9d–9f, this so-called layer-polarization-induced polarizing field has been predicted to stabilize a net polarization in ultrathin (001)-oriented KTaO_3 films.¹²⁹ Here, the formal K^{+1} , Ta^{5+} and O^{2-} in KTaO_3 lead to positive $[\text{TaO}_2]^{+1}$ and negative $[\text{KO}]^{-1}$ planes as shown in the Figure 9e and 9f.

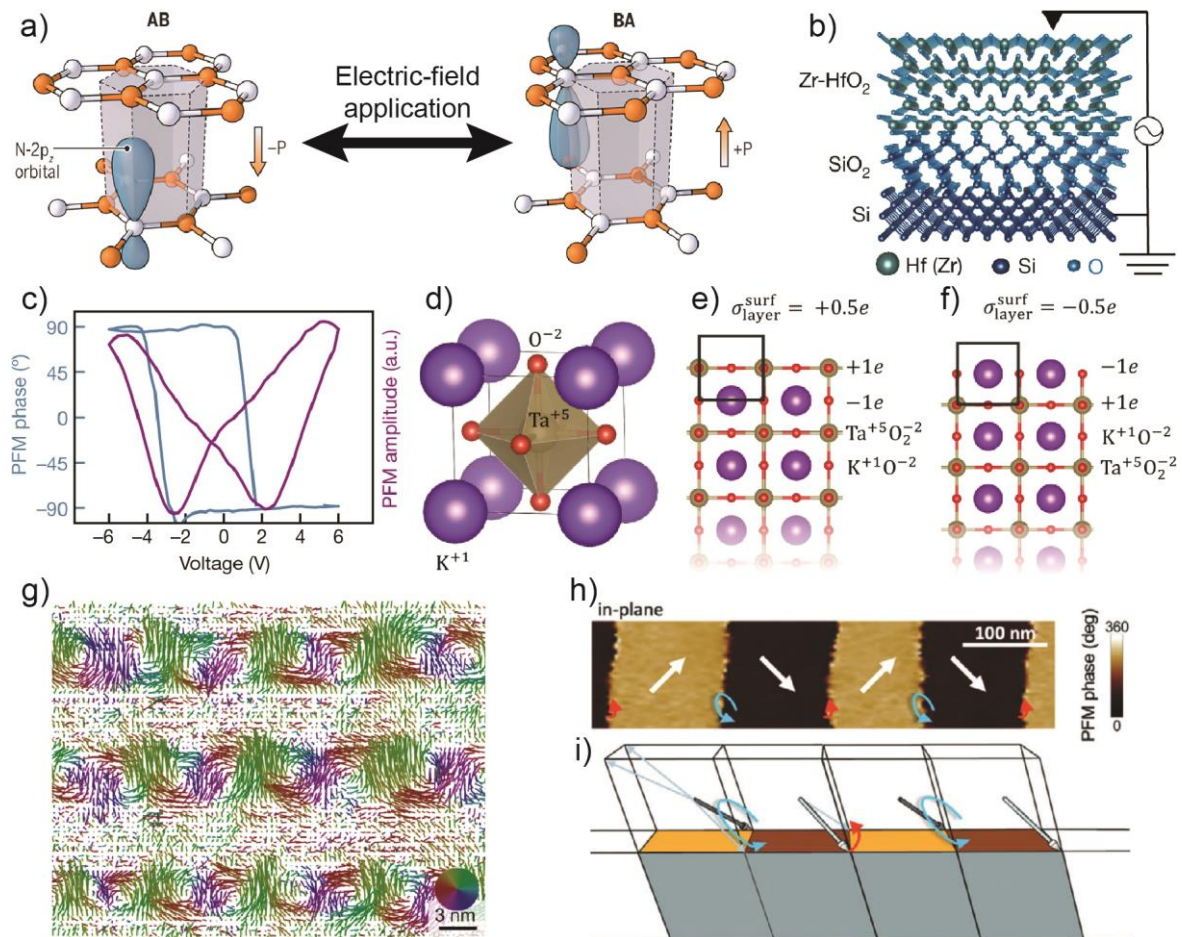


Figure 9: Emerging concepts to overcome the issue of polarization suppression in the ultrathin regime. a) Illustration of the sliding ferroelectricity in a double layer of $h\text{-BN}$. The out-of-plane polarization emerges as a result of the non-centrosymmetric AB/BA stacking of the two $h\text{-BN}$ monolayers. Reproduced with permission from ¹⁰⁵, copyright (2021) by AAAS. b) and c) Demonstration of a switchable ferroelectric polarization in 1 nm thick Zr-doped HfO_2 films on SiO_2 -buffered Si. Reproduced with permission from ¹²⁰, copyright (2020) by Springer Nature. d)–f) Illustration of the concept of layer polarization for the example of KTaO_3 . In ultrathin films the polarizing field due to the lattice polarization has been predicted to induce a net polarization. Reproduced with permission from ¹²⁹, copyright (2022) by the American Physical Society. g) STEM map of the dipole moments in a $\text{PbTiO}_3|\text{SrTiO}_3$ superlattice. Reproduced with permission from ⁶⁴, copyright (2019) by AAAS. h) and i) Piezoresponse force microscopy image and the corresponding three-dimensional graphical illustration showing the chiral domain walls in BiFeO_3 films with a stripe domain structure. Reproduced with permissions from ¹³⁰, copyright (2022) by John Wiley and Sons.

5.4 Polar chirality and the electric equivalent to the magnetic Dzyaloshinskii–Moriya interaction

The interest in non-collinear arrangements of electric dipoles, similar to the one depicted in Figure 9g, was sparked by the experimental reports of topological textures in ferroelectric thin-films and superlattices.¹³¹ Such complex electric dipole orderings open new avenues in both fundamental and applied research communities. The advances in transmission electron microscopy, scanning probe microscopy, and SHG analysis of thin films led to the observation of nanoscale polar bubble domains, non-Ising domain walls^{37,78}, polar vortices, flux closure domains, polar skyrmions, and merons. All these textures hold promises for energy efficient data storage possibilities. For a long time, rotational profiles in the polarization were deemed to be energetically unfavorable due to the strong lattice-polarization coupling that led to the prediction of exclusively Ising-like dipole configurations. Extensive research efforts in the last decade, however, showcased the dominating role of electrostatic and elastic boundary conditions in setting the final polarization states in ultrathin oxide heterostructures and supporting the emergence of exotic polar topologies.¹³¹

The report of a net chirality in the ordering of polar vortices further rendered polar chirality as potential additional degree of freedom in the design of functional ferroelectric systems. Chirality is a concept central to the chemical structure of molecules, but it became a crucial component in condensed matter physics, as well. In particular, in ferromagnetic metals¹³² and ferrimagnetic insulators^{133,134}, homochiral domain walls were shown to enable deterministic current-driven domain-wall motion. In such systems, the stabilization of a net chirality at magnetic domain walls is usually the consequence of the Dzyaloshinskii-Moriya interaction¹³⁵, which is an antisymmetric magnetic exchange interaction. It can promote a canting of the spin ordering and drive the sense of rotation of the magnetic order parameter across the domain walls. For a long time, it was assumed that the DMI, that is characteristic for magnetically ordered systems, had no equivalent phenomenon in electrically ordered materials.¹³⁶ However, recent reports based on symmetry analysis and first-principles calculations have now predicted such electrical DM-like terms in a number of ferroelectric and antiferroelectric perovskite oxides as one of the symmetry-allowed energetic couplings.⁷⁹ While the electric DM-like interaction has a one-to-one correspondence with the magnetic DMI in terms of symmetry considerations, from a phenomenological standpoint its physical origin is fundamentally different.⁷⁹ In perovskite oxides, the polar DM-like interaction is argued to arise from the trilinear interaction between oxygen-octahedral tilt patterns⁷⁹. Trilinear coupling mechanisms can arise not only in the bulk of a material as demonstrated with density-functional theory calculations⁷⁹, but can likely also originate from interfaces. Interestingly, the emergence of 'hybrid improper ferroelectricity' in $\text{PbTiO}_3|\text{SrTiO}_3$ multilayers is also explained by a trilinear term arising at interfaces that couples two non-polar distortions and triggers a polar distortion¹³⁷ as a result, suggesting the possibility to stabilize electric DM-like interaction in complex oxide heterostructures too. Likely the first experimental signature of electric DMI in ferroelectric films showed that the formation of homochiral domain walls in BiFeO_3 can be triggered by the symmetry breaking provided by an in-plane-polarized buffer layer.¹⁰³ Similarly, the symmetry breaking associated with the periodically striped ferroelectric domain pattern in BiFeO_3 was suggested as the origin for chiral domain-wall textures (Figures 9h and 9i).^{130,138}

6. CONCLUSION AND OUTLOOK

In this spotlight on applications, we presented the recent developments on ferroelectricity in ultrathin films and introduced most recent device concepts involving ferroelectric materials. Characterization tools giving access to buried polarization states such as tomographic AFM and APT promise further advances in the understanding of the role of interfaces on the final polarization state of the films once inserted into a device architecture. We then highlighted the studies involving in-situ non-linear optics which provide unprecedented capabilities for non-invasive characterizations of polar states. Optical SHG is compatible with operando investigations and further offers the prospect for additional time-resolved measurements. In particular, the dynamics of ultrathin ferroelectric or multiferroic films may be explored in application-relevant integrated configurations. Most importantly, the direct access to the polarization during the growth will be key in the design of emerging oxide electronic devices based on electrically ordered materials. So far, studies revealed the existence of transient states during the growth that could lead to new design capacities. As a result, interface synergy and controlled domain formation were engineered in films for improved ferroelectric responses. Beyond the perovskite materials, the work on Aurivillius compounds demonstrated the ability to develop high-precision design of complex layered oxide thin-films. Finally, we provided some insights in emerging fields and materials for nanoscale ferroelectricity. In particular, the control of chiral configurations in ferroelectrics is still a field in its infancy, calling for further investigations allowing to unambiguously connect the experimental observations to the exact physical origins driving them. Once established, it could be utilized to enable a uniform domain-wall motion under applied electric fields or to stabilize electric skyrmions in ferroelectric materials.

7. ACKNOWLEDGMENTS

We acknowledge the Swiss National Science Foundation under Project No. 200021-188414 and the Swiss National Science Foundation Spark funding CRSK-2_196061. All authors thank Manfred Fiebig for financial support.

Bibliography

- (1) Rabe, K.; Ahn, C.; Triscone, J. Physics of Ferroelectrics. *Springer* **2007**, 105 (2007), 1.
- (2) Strkalj, N.; Gradauskaite, E.; Nordlander, J.; Trassin, M. Design and Manipulation of Ferroic Domains in Complex Oxide Heterostructures. *Materials (Basel)*. **2019**, 12 (19), 3108. <https://doi.org/10.3390/MA12193108>.
- (3) Rödel, J.; Jo, W.; Seifert, K. T. P.; Anton, E. M.; Granzow, T.; Damjanovic, D. Perspective on the Development of Lead-Free Piezoceramics. *J. Am. Ceram. Soc.* **2009**, 92 (6), 1153–1177. <https://doi.org/10.1111/J.1551-2916.2009.03061.X>.
- (4) Setter, N.; Damjanovic, D.; Eng, L.; Fox, G.; Gevorgian, S.; Hong, S.; Kingon, A.; Kohlstedt, H.; Park, N. Y.; Stephenson, G. B.; Stolitchnov, I.; TagansteV, A. K.; Taylor, D. V.; Yamada, T.; Streiffer, S. Ferroelectric Thin Films: Review of Materials, Properties, and Applications. *J. Appl. Phys.* **2006**, 100 (5), 051606. <https://doi.org/10.1063/1.2336999>.
- (5) Fiebig, M.; Lottermoser, T.; Meier, D.; Trassin, M. The Evolution of Multiferroics. *Nat. Rev. Mater.* **2016**, 1 (8), 16046. <https://doi.org/10.1038/natrevmats.2016.46>.
- (6) Van Aken, B. B.; Palstra, T. T. M.; Filippetti, A.; Spaldin, N. A. The Origin of Ferroelectricity in Magnetoelectric YMnO₃. *Nat. Mater.* **2004**, 3 (3), 164–170. <https://doi.org/10.1038/nmat1080>.
- (7) Meier, D.; Seidel, J.; Cano, A.; Delaney, K.; Kumagai, Y.; Mostovoy, M.; Spaldin, N. A.; Ramesh, R.; Fiebig, M. Anisotropic Conductance at Improper Ferroelectric Domain Walls. *Nat. Mater.* **2012**, 11 (4), 284–288. <https://doi.org/10.1038/nmat3249>.
- (8) Trassin, M.; Garcia, V. Bringing Some Bulk into Ferroelectric Devices. *Nat. Mater.* **2022**, 21 (7), 730–731. <https://doi.org/10.1038/s41563-022-01267-5>.
- (9) De Luca, G.; Strkalj, N.; Manz, S.; Bouillet, C.; Fiebig, M.; Trassin, M. Nanoscale Design of Polarization in Ultrathin Ferroelectric Heterostructures. *Nat. Commun.* **2017**, 8 (1), 1419. <https://doi.org/10.1038/s41467-017-01620-2>.
- (10) Strkalj, N.; De Luca, G.; Campanini, M.; Pal, S.; Schaab, J.; Gattinoni, C.; Spaldin, N. A.; Rossell, M. D.; Fiebig, M.; Trassin, M. Depolarizing Field Effects in Epitaxial Capacitor Heterostructures. *Phys. Rev. Lett.* **2019**, 123 (14), 147601. <https://doi.org/10.1103/PhysRevLett.123.147601>.
- (11) Steffes, J. J.; Ristau, R. A.; Ramesh, R.; Huey, B. D. Thickness Scaling of Ferroelectricity in BiFeO₃ by Tomographic Atomic Force Microscopy. *Proc. Natl. Acad. Sci. U. S. A.* **2019**, 116 (7), 2413–2418. <https://doi.org/10.1073/pnas.1806074116>.
- (12) Nordlander, J.; Campanini, M.; Rossell, M. D.; Erni, R.; Meier, Q. N.; Cano, A.; Spaldin, N. A.; Fiebig, M.; Trassin, M. The Ultrathin Limit of Improper Ferroelectricity. *Nat. Commun.* **2019**, 10 (1), 1–7. <https://doi.org/10.1038/s41467-019-13474-x>.
- (13) Lichtensteiger, C.; Triscone, J. M.; Junquera, J.; Ghosez, P. Ferroelectricity

- and Tetragonality in Ultrathin PbTiO₃ Films. *Phys. Rev. Lett.* **2005**, *94* (4), 047603.
<https://doi.org/10.1103/PHYSREVLETT.94.047603/FIGURES/3/MEDIUM>.
- (14) Choi, K. J.; Biegalski, M.; Li, Y. L.; Sharan, A.; Schubert, J.; Uecker, R.; Reiche, P.; Chen, Y. B.; Pan, X. Q.; Gopalan, V.; Che, L. Q.; Schlom, D. C.; Eom, C. B. Enhancement of Ferroelectricity in Strained BaTiO₃ Thin Films. *Science* (80-.). **2004**, *306* (5698), 1005–1009.
https://doi.org/10.1126/SCIENCE.1103218/SUPPL_FILE/CHOI.SOM.PDF.
- (15) Ederer, C.; Spaldin, N. A. Effect of Epitaxial Strain on the Spontaneous Polarization of Thin Film Ferroelectrics. *Phys. Rev. Lett.* **2005**, *95* (25), 257601.
<https://doi.org/10.1103/PHYSREVLETT.95.257601/FIGURES/2/MEDIUM>.
- (16) Chen, B.; Gauquelin, N.; Strkalj, N.; Huang, S.; Halisdemir, U.; Nguyen, M. D.; Jannis, D.; Sarott, M. F.; Eltes, F.; Abel, S.; Spreitzer, M.; Fiebig, M.; Trassin, M.; Fompeyrine, J.; Verbeeck, J.; Huijben, M.; Rijnders, G.; Koster, G. Signatures of Enhanced Out-of-Plane Polarization in Asymmetric BaTiO₃ Superlattices Integrated on Silicon. *Nat. Commun.* **2022**, *13* (1), 1–8.
<https://doi.org/10.1038/s41467-021-27898-x>.
- (17) Kormondy, K. J.; Popoff, Y.; Sousa, M.; Eltes, F.; Caimi, D.; Rossell, M. D.; Fiebig, M.; Hoffmann, P.; Marchiori, C.; Reinke, M.; Trassin, M.; Demkov, A. A.; Fompeyrine, J.; Abel, S. Microstructure and Ferroelectricity of BaTiO₃ Thin Films on Si for Integrated Photonics. *Nanotechnology* **2017**, *28* (7), 075706.
<https://doi.org/10.1088/1361-6528/AA53C2>.
- (18) Nordlander, J.; Eltes, F.; Reynaud, M.; Nürnberg, J.; De Luca, G.; Caimi, D.; Demkov, A. A.; Abel, S.; Fiebig, M.; Fompeyrine, J.; Trassin, M. Ferroelectric Domain Architecture and Poling of BaTiO₃ on Si. *Phys. Rev. Mater.* **2020**, *4* (3), 034406. <https://doi.org/10.1103/PhysRevMaterials.4.034406>.
- (19) Manipatruni, S.; Nikonov, D. E.; Lin, C. C.; Gosavi, T. A.; Liu, H.; Prasad, B.; Huang, Y. L.; Bonturim, E.; Ramesh, R.; Young, I. A. Scalable Energy-Efficient Magnetoelectric Spin–Orbit Logic. *Nature* **2019**, *565* (7737), 35–42.
<https://doi.org/10.1038/s41586-018-0770-2>.
- (20) Salahuddin, S.; Datta, S. Use of Negative Capacitance to Provide Voltage Amplification for Low Power Nanoscale Devices. *Nano Lett.* **2008**, *8* (2), 405–410.
https://doi.org/10.1021/NL071804G/SUPPL_FILE/NL071804GSI20071003_094513.PDF.
- (21) Trassin, M. Low Energy Consumption Spintronics Using Multiferroic Heterostructures. *J. Phys. Condens. Matter* **2016**, *28* (3), 033001.
<https://doi.org/10.1088/0953-8984/28/3/033001>.
- (22) Heron, J. T.; Bosse, J. L.; He, Q.; Gao, Y.; Trassin, M.; Ye, L.; Clarkson, J. D.; Wang, C.; Liu, J.; Salahuddin, S.; Ralph, D. C.; Schlom, D. G.; Íñiguez, J.; Huey, B. D.; Ramesh, R. Deterministic Switching of Ferromagnetism at Room Temperature Using an Electric Field. *Nature* **2014**, *516* (7531), 370–373.
<https://doi.org/10.1038/nature14004>.
- (23) Müller, M.; Huang, Y.; Vélez, S.; Ramesh, R.; Fiebig, M.; Trassin, M. Training the Polarization in Integrated La_{0.15}Bi_{0.85}FeO₃-Based Devices. *Adv.*

Mater. **2021**, 2104688. <https://doi.org/10.1002/adma.202104688>.

- (24) Liu, G.; Zhang, S.; Jiang, W.; Cao, W. Losses in Ferroelectric Materials. *Materials Science and Engineering R: Reports*. Elsevier Ltd March 1, 2015, pp 1–48. <https://doi.org/10.1016/j.mser.2015.01.002>.
- (25) Malyshkina, O.; Eliseev, A.; Grechishkin, R. Heat Losses in Ferroelectric Ceramics Due to Switching Processes. *Proc. Est. Acad. Sci.* **2017**, 66 (4), 462–466. <https://doi.org/10.3176/proc.2017.4.07>.
- (26) Kim, J. Y.; Choi, M. J.; Jang, H. W. Ferroelectric Field Effect Transistors: Progress and Perspective. *APL Mater.* **2021**, 9 (2), 021102. <https://doi.org/10.1063/5.0035515>.
- (27) Landauer, R. Can Capacitance Be Negative? *Collect. Phenom.* **1976**, 2, 167–170.
- (28) Saha, A. K.; Gupta, S. K. Negative Capacitance Effects in Ferroelectric Heterostructures: A Theoretical Perspective. *J. Appl. Phys.* **2021**, 129 (8). <https://doi.org/10.1063/5.0038971>.
- (29) Islam Khan, A.; Bhowmik, D.; Yu, P.; Joo Kim, S.; Pan, X.; Ramesh, R.; Salahuddin, S. Experimental Evidence of Ferroelectric Negative Capacitance in Nanoscale Heterostructures. *Appl. Phys. Lett.* **2011**, 99 (11), 113501. <https://doi.org/10.1063/1.3634072>.
- (30) Cheema, S. S.; Shanker, N.; Hsu, C. H.; Datar, A.; Bae, J.; Kwon, D.; Salahuddin, S. One Nanometer HfO₂-Based Ferroelectric Tunnel Junctions on Silicon. *Adv. Electron. Mater.* **2022**, 8 (6), 1–10. <https://doi.org/10.1002/aelm.202100499>.
- (31) Garcia, V.; Fusil, S.; Bouzehouane, K.; Enouz-Vedrenne, S.; Mathur, N. D.; Barthélémy, A.; Bibes, M. Giant Tunnel Electroresistance for Non-Destructive Readout of Ferroelectric States. *Nat. 2009 4607251* **2009**, 460 (7251), 81–84. <https://doi.org/10.1038/nature08128>.
- (32) Asif, M.; Kumar, A. Resistive Switching in Emerging Materials and Their Characteristics for Neuromorphic Computing. *Mater. Today Electron.* **2022**, 1, 100004. <https://doi.org/10.1016/j.mtelec.2022.100004>.
- (33) Zidan, M. A.; Strachan, J. P.; Lu, W. D. The Future of Electronics Based on Memristive Systems. *Nat. Electron. 2017 11* **2018**, 1 (1), 22–29. <https://doi.org/10.1038/s41928-017-0006-8>.
- (34) Garcia, V.; Bibes, M. Ferroelectric Tunnel Junctions for Information Storage and Processing. *Nat. Commun. 2014 51* **2014**, 5 (1), 1–12. <https://doi.org/10.1038/ncomms5289>.
- (35) Seidel, J.; Martin, L. W.; He, Q.; Zhan, Q.; Chu, Y.-H.; Rother, A.; Hawkrigde, M. E.; Maksymovych, P.; Yu, P.; Gajek, M.; Balke, N.; Kalinin, S. V.; Gemming, S.; Wang, F.; Catalan, G.; Scott, J. F.; Spaldin, N. A.; Orenstein, J.; Ramesh, R. Conduction at Domain Walls in Oxide Multiferroics. *Nat. Mater.* **2009**, 8 (3), 229–234. <https://doi.org/10.1038/nmat2373>.
- (36) Guyonnet, J.; Gaponenko, I.; Gariglio, S.; Paruch, P. Conduction at Domain Walls in Insulating Pb(Zr_{0.2}Ti_{0.8})O₃ Thin Films. *Adv. Mater.* **2011**, 23 (45), 5377–5382. <https://doi.org/10.1002/ADMA.201102254>.

- (37) De Luca, G.; Rossell, M. D.; Schaab, J.; Viart, N.; Fiebig, M.; Trassin, M.; De Luca, G.; Schaab, J.; Fiebig, M.; Trassin, M.; Rossell, M. D.; Viart, N. Domain Wall Architecture in Tetragonal Ferroelectric Thin Films. *Adv. Mater.* **2017**, *29* (7), 1605145. <https://doi.org/10.1002/ADMA.201605145>.
- (38) Meier, D.; Selbach, S. M. Ferroelectric Domain Walls for Nanotechnology. *Nat. Rev. Mater.* **2021**, *7* (3), 157–173. <https://doi.org/10.1038/s41578-021-00375-z>.
- (39) Varotto, S.; Nessi, L.; Cecchi, S.; Sławińska, J.; Noël, P.; Petrò, S.; Fagiani, F.; Novati, A.; Cantoni, M.; Petti, D.; Albisetti, E.; Costa, M.; Calarco, R.; Buongiorno Nardelli, M.; Bibes, M.; Picozzi, S.; Attané, J. P.; Vila, L.; Bertacco, R.; Rinaldi, C. Room-Temperature Ferroelectric Switching of Spin-to-Charge Conversion in Germanium Telluride. *Nat. Electron.* **2021**, *4* (10), 740–747. <https://doi.org/10.1038/s41928-021-00653-2>.
- (40) Strkalj, N.; De Luca, G.; Campanini, M.; Pal, S.; Schaab, J.; Gattinoni, C.; Spaldin, N. A.; Rossell, M. D.; Fiebig, M.; Trassin, M. Depolarizing-Field Effects in Epitaxial Capacitor Heterostructures. *Phys. Rev. Lett.* **2019**, *123* (14), 147601. <https://doi.org/10.1103/PhysRevLett.123.147601>.
- (41) Ilev, A. V.; Maksymovych, P.; Trassin, M.; Seidel, J.; Ramesh, R.; Kalinin, S. V.; Ovchinnikova, O. S. Chemical State Evolution in Ferroelectric Films during Tip-Induced Polarization and Electroresistive Switching. *ACS Appl. Mater. Interfaces* **2016**, *8* (43), 29588–29593. https://doi.org/10.1021/ACSAMI.6B10784/ASSET/IMAGES/LARGE/AM-2016-10784Z_0005.JPEG.
- (42) Campanini, M.; Gradauskaite, E.; Trassin, M.; Yi, D.; Yu, P.; Ramesh, R.; Erni, R.; Rossell, M. D. Imaging and Quantification of Charged Domain Walls in BiFeO₃. *Nanoscale* **2020**, *12* (16), 9186–9193. <https://doi.org/10.1039/D0NR01258K>.
- (43) Unguris, J.; Bowden, S. R.; Pierce, D. T.; Trassin, M.; Ramesh, R.; Cheong, S. W.; Fackler, S.; Takeuchi, I. Simultaneous Imaging of the Ferromagnetic and Ferroelectric Structure in Multiferroic Heterostructures. *APL Mater.* **2014**, *2* (7), 076109. <https://doi.org/10.1063/1.4890055>.
- (44) Sarott, M. F.; Gradauskaite, E.; Nordlander, J.; Strkalj, N.; Trassin, M. In Situ Monitoring of Epitaxial Ferroelectric Thin-Film Growth. *J. Phys. Condens. Matter* **2021**, *33* (29), 293001. <https://doi.org/10.1088/1361-648X/ABF979>.
- (45) Schmitz, J. Low Temperature Thin Films for Next-Generation Microelectronics (Invited). *Surf. Coatings Technol.* **2018**, *343*, 83–88. <https://doi.org/10.1016/j.surfcoat.2017.11.013>.
- (46) Mikolajick, T.; Slesazek, S.; Mulaosmanovic, H.; Park, M. H.; Fichtner, S.; Lomenzo, P. D.; Hoffmann, M.; Schroeder, U. Next Generation Ferroelectric Materials for Semiconductor Process Integration and Their Applications. *J. Appl. Phys.* **2021**, *129* (10), 100901. <https://doi.org/10.1063/5.0037617>.
- (47) Trassin, M.; De Luca, G.; Manz, S.; Fiebig, M. Probing Ferroelectric Domain Engineering in BiFeO₃ Thin Films by Second Harmonic Generation. *Adv. Mater.* **2015**, *27* (33), 4871–4876. <https://doi.org/10.1002/adma.201501636>.

- (48) De Luca, G.; Schoenherr, P.; Mendil, J.; Meier, D.; Fiebig, M.; Trassin, M. Domain-Pattern Transfer across an Artificial Magnetoelectric Interface. *Phys. Rev. Appl.* **2018**, *10* (5), 054030. <https://doi.org/10.1103/PhysRevApplied.10.054030>.
- (49) Song, J.; Zhou, Y.; Huey, B. D. 3D Structure–Property Correlations of Electronic and Energy Materials by Tomographic Atomic Force Microscopy. *Appl. Phys. Lett.* **2021**, *118* (8), 80501. <https://doi.org/10.1063/5.0040984>.
- (50) Kim, Y.; Lieber, C. M. Machining Oxide Thin Films with an Atomic Force Microscope: Pattern and Object Formation on the Nanometer Scale. *Science* (80-.). **1992**, *257* (5068), 375–377. <https://doi.org/10.1126/science.257.5068.375>.
- (51) Steffes, J. J.; Ristau, R. A.; Ramesh, R.; Huey, B. D. Thickness Scaling of Ferroelectricity in BiFeO₃ by Tomographic Atomic Force Microscopy. *Proc. Natl. Acad. Sci. U. S. A.* **2019**, *116* (7), 2413–2418. <https://doi.org/10.1073/pnas.1806074116>.
- (52) Gault, B.; Chiaramonti, A.; Cojocaru-Mirédin, O.; Stender, P.; Dubosq, R.; Freysoldt, C.; Makineni, S. K.; Li, T.; Moody, M.; Cairney, J. M. Atom Probe Tomography. *Nat. Rev. Methods Prim.* **2021**, *1* (1), 51. <https://doi.org/10.1038/s43586-021-00047-w>.
- (53) Kirchhofer, R.; Diercks, D. R.; Gorman, B. P.; Ihlefeld, J. F.; Kotula, P. G.; Shelton, C. T.; Brennecke, G. L. Quantifying Compositional Homogeneity in Pb(Zr,Ti)O₃ Using Atom Probe Tomography. *J. Am. Ceram. Soc.* **2014**, *97* (9), 2677–2697. <https://doi.org/https://doi.org/10.1111/jace.13135>.
- (54) Kelly, T. F.; Vella, A.; Bunton, J. H.; Houard, J.; Silaeva, E. P.; Bogdanowicz, J.; Vandervorst, W. Laser Pulsing of Field Evaporation in Atom Probe Tomography. *Curr. Opin. Solid State Mater. Sci.* **2014**, *18* (2), 81–89. <https://doi.org/https://doi.org/10.1016/j.cossms.2013.11.001>.
- (55) Xu, X.; Liu, Y.; Wang, J.; Isheim, D.; Dravid, V. P.; Phatak, C.; Haile, S. M. Variability and Origins of Grain Boundary Electric Potential Detected by Electron Holography and Atom-Probe Tomography. *Nat. Mater.* **2020**, *19* (8), 887–893. <https://doi.org/10.1038/s41563-020-0656-1>.
- (56) Gradauskaite, E.; Hunnestad, K. A.; Meier, Q. N.; Meier, D.; Trassin, M. Ferroelectric Domain Engineering Using Structural Defect Ordering. *Chem. Mater.* **2022**, *34* (14), 6468–6475. <https://doi.org/10.1021/acs.chemmater.2c01178>.
- (57) Hunnestad, K. A.; Hatzoglou, C.; Khalid, Z. M.; Vullum, P. E.; Yan, Z.; Bourret, E.; van Helvoort, A. T. J.; Selbach, S. M.; Meier, D. Atomic-Scale 3D Imaging of Individual Dopant Atoms in a Complex Oxide. **2021**, 1–7. <https://doi.org/10.1038/s41467-022-32189-0>.
- (58) Fong, D. D.; Thompson, C. IN SITU SYNCHROTRON X-RAY STUDIES OF FERROELECTRIC THIN FILMS. <https://doi.org/10.1146/annurev.matsci.36.090804.100242> **2006**, *36*, 431–465. <https://doi.org/10.1146/ANNUREV.MATSCI.36.090804.100242>.
- (59) Denev, S. A.; Lummen, T. T. A.; Barnes, E.; Kumar, A.; Gopalan, V. Probing Ferroelectrics Using Optical Second Harmonic Generation. *J. Am. Ceram. Soc.*

- 2011, 94 (9), 2699–2727. <https://doi.org/10.1111/j.1551-2916.2011.04740.x>.
- (60) Fiebig, M.; Pavlov, V. V.; Pisarev, R. V. Second-Harmonic Generation as a Tool for Studying Electronic and Magnetic Structures of Crystals: Review. *J. Opt. Soc. Am. B* **2005**, 22 (1), 96. <https://doi.org/10.1364/JOSAB.22.000096>.
- (61) Timpu, F.; Reig Escalé, M.; Timofeeva, M.; Strkalj, N.; Trassin, M.; Fiebig, M.; Grange, R.; Timpu, F.; Reig Escalé, M.; Timofeeva, M.; Grange, R.; Strkalj, N.; Trassin, M.; Fiebig, M. Enhanced Nonlinear Yield from Barium Titanate Metasurface Down to the Near Ultraviolet. *Adv. Opt. Mater.* **2019**, 7 (22), 1900936. <https://doi.org/10.1002/ADOM.201900936>.
- (62) Homkar, S.; Preziosi, D.; Devaux, X.; Bouillet, C.; Nordlander, J.; Trassin, M.; Roulland, F.; Lefèvre, C.; Versini, G.; Barre, S.; Leuvrey, C.; Lenertz, M.; Fiebig, M.; Pourroy, G.; Viart, N. Ultrathin Regime Growth of Atomically Flat Multiferroic Gallium Ferrite Films with Perpendicular Magnetic Anisotropy. *Phys. Rev. Mater.* **2019**, 3 (12), 124416. <https://doi.org/10.1103/PHYSREVMATERIALS.3.124416>/FIGURES/8/MEDIUM .
- (63) Nordlander, J.; Rossell, M. D.; Campanini, M.; Fiebig, M.; Trassin, M. Epitaxial Integration of Improper Ferroelectric Hexagonal YMnO₃ Thin Films in Heterostructures. *Phys. Rev. Mater.* **2020**, 4 (12), 124403. <https://doi.org/10.1103/PHYSREVMATERIALS.4.124403>/FIGURES/6/MEDIUM .
- (64) Strkalj, N.; Bortis, A.; Campanini, M.; Rossell, M. D.; Fiebig, M.; Trassin, M. Optical Second Harmonic Signature of Phase Coexistence in Ferroelectric/dielectric Heterostructures. *Phys. Rev. B* **2022**, 105 (17), 174101. <https://doi.org/10.1103/PHYSREVB.105.174101>/FIGURES/5/MEDIUM.
- (65) Nordlander, J.; Rossell, M. D.; Campanini, M.; Fiebig, M.; Trassin, M. Inversion-Symmetry Engineering in Layered Oxide Thin Films. *Nano Lett.* **2021**, 21 (7), 2780–2785. <https://doi.org/10.1021/ACS.NANOLETT.0C04819>/ASSET/IMAGES/LARGE/NL0C04819_0004.JPEG.
- (66) Nordlander, J.; Luca, G. De; Strkalj, N.; Fiebig, M.; Trassin, M.; Nordlander, J.; De Luca, G.; Strkalj, N.; Fiebig, M.; Trassin, M. Probing Ferroic States in Oxide Thin Films Using Optical Second Harmonic Generation. *Appl. Sci.* **2018**, 8 (4), 570. <https://doi.org/10.3390/app8040570>.
- (67) Neacsu, C. C.; Van Aken, B. B.; Fiebig, M.; Raschke, M. B. Second-Harmonic near-Field Imaging of Ferroelectric Domain Structure of YMnO₃. *Phys. Rev. B - Condens. Matter Mater. Phys.* **2009**, 79 (10), 100107. <https://doi.org/10.1103/PhysRevB.79.100107>.
- (68) Ihlefeld, J. F.; Michael, J. R.; McKenzie, B. B.; Scrymgeour, D. A.; Maria, J. P.; Paisley, E. A.; Kitahara, A. R. Domain Imaging in Ferroelectric Thin Films via Channeling-Contrast Backscattered Electron Microscopy. *J. Mater. Sci.* **2017**, 52 (2), 1071–1081. <https://doi.org/10.1007/s10853-016-0402-x>.
- (69) Zhang, Y.; Tan, Y.; Sando, D.; Chen, L.; Valanoor, N.; Zhu, Y.; Han, M. Controlled Nucleation and Stabilization of Ferroelectric Domain Wall Patterns in Epitaxial (110) Bismuth Ferrite Heterostructures. *Adv. Funct. Mater.* **2020**,

2003571. <https://doi.org/10.1002/adfm.202003571>.

- (70) Vogel, A.; Sarott, M. F.; Campanini, M.; Trassin, M.; Rossell, M. D. Monitoring Electrical Biasing of Pb(Zr_{0.2}Ti_{0.8})O₃ Ferroelectric Thin Films in Situ by Dpc-Stem Imaging. *Materials (Basel)*. **2021**, *14* (16), 4749. <https://doi.org/10.3390/MA14164749/S1>.
- (71) Weber, M. C.; Zemp, Y.; Trassin, M.; Simonov, A.; Schaab, J.; Gao, B.; Cheong, S. W.; Lottermoser, T.; Fiebig, M. Asymmetric Character of the Ferroelectric Phase Transition and Charged Domain Walls in a Hybrid Improper Ferroelectric. *Adv. Electron. Mater.* **2022**, *8* (6), 2100434. <https://doi.org/10.1002/AELM.202100434>.
- (72) Shimamoto, K.; Mukherjee, S.; Manz, S.; White, J. S.; Trassin, M.; Kenzelmann, M.; Chapon, L.; Lippert, T.; Fiebig, M.; Schneider, C. W.; Niedermayer, C. Tuning the Multiferroic Mechanisms of TbMnO₃ by Epitaxial Strain. *Sci. Reports 2017 71* **2017**, *7* (1), 1–9. <https://doi.org/10.1038/srep44753>.
- (73) Trassin, M.; Viart, N.; Versini, G.; Barre, S.; Pourroy, G.; Lee, J.; Jo, W.; Dumesnil, K.; Dufour, C.; Robert, S. Room Temperature Ferrimagnetic Thin Films of the Magnetoelectric Ga_{2-x}Fe_xO₃. *J. Mater. Chem.* **2009**, *19* (46), 8876–8880. <https://doi.org/10.1039/B913359C>.
- (74) Trassin, M.; Viart, N.; Versini, G.; Loison, J. L.; Vola, J. P.; Schmerber, G.; Crgut, O.; Barre, S.; Pourroy, G.; Lee, J. H.; Jo, W.; Mny, C. Epitaxial Thin Films of Multiferroic GaFeO₃ on Conducting Indium Tin Oxide (001) Buffered Yttrium-Stabilized Zirconia (001) by Pulsed Laser Deposition. *Appl. Phys. Lett.* **2007**, *91* (20), 202504. <https://doi.org/10.1063/1.2813020>.
- (75) Zhou, Z.; Trassin, M.; Gao, Y.; Gao, Y.; Qiu, D.; Ashraf, K.; Nan, T.; Yang, X.; Bowden, S. R.; Pierce, D. T.; Stiles, M. D.; Unguris, J.; Liu, M.; Howe, B. M.; Brown, G. J.; Salahuddin, S.; Ramesh, R.; Sun, N. X. Probing Electric Field Control of Magnetism Using Ferromagnetic Resonance. *Nat. Commun.* **2015**, *6* (1), 6082. <https://doi.org/10.1038/ncomms7082>.
- (76) Heron, J. T.; Trassin, M.; Ashraf, K.; Gajek, M.; He, Q.; Yang, S. Y.; Nikonov, D. E.; Chu, Y.-H.; Salahuddin, S.; Ramesh, R. Electric-Field-Induced Magnetization Reversal in a Ferromagnet-Multiferroic Heterostructure. *Phys. Rev. Lett.* **2011**, *107* (21), 217202. <https://doi.org/10.1103/PhysRevLett.107.217202>.
- (77) Trassin, M.; Clarkson, J. D.; Bowden, S. R.; Liu, J.; Heron, J. T.; Paull, R. J.; Arenholz, E.; Pierce, D. T.; Unguris, J. Interfacial Coupling in Multiferroic/Ferromagnet Heterostructures. *Phys. Rev. B* **2013**, *87* (13), 134426. <https://doi.org/10.1103/PhysRevB.87.134426>.
- (78) Cherifi-Hertel, S.; Bulou, H.; Hertel, R.; Taupier, G.; Dorkenoo, K. D. H.; Andreas, C.; Guyonnet, J.; Gaponenko, I.; Gallo, K.; Paruch, P. Non-Ising and Chiral Ferroelectric Domain Walls Revealed by Nonlinear Optical Microscopy. *Nat. Commun.* **2017**, *8*. <https://doi.org/10.1038/ncomms15768>.
- (79) Zhao, H. J.; Chen, P.; Prosandeev, S.; Artyukhin, S.; Bellaiche, L. Dzyaloshinskii–Moriya-like Interaction in Ferroelectrics and Antiferroelectrics. *Nat. Mater.* **2021**, *20* (3), 341–345. <https://doi.org/10.1038/s41563-020-00821->

3.

- (80) Jähnke, V.; Conrad, U.; Gütde, J.; Matthias, E. SHG Investigations of the Magnetization of Thin Ni and Co Films on Cu(001). *Appl. Phys. B* **1999**, *68* (3), 485–489. <https://doi.org/10.1007/S003400050653>.
- (81) Jin, Q. Y.; Regensburger, H.; Vollmer, R.; Kirschner, J. Periodic Oscillations of the Surface Magnetization during the Growth of Co Films on Cu(001). *Phys. Rev. Lett.* **1998**, *80* (18), 4056. <https://doi.org/10.1103/PhysRevLett.80.4056>.
- (82) Rubano, A.; Günter, T.; Lilienblum, M.; Aruta, C.; Miletto Granozio, F.; Scotti Di Uccio, U.; Marrucci, L.; Paparo, D.; Fiebig, M. Optical Second Harmonic Imaging as a Diagnostic Tool for Monitoring Epitaxial Oxide Thin-Film Growth. *Appl. Surf. Sci.* **2015**, *327*, 413–417. <https://doi.org/10.1016/J.APSUSC.2014.11.051>.
- (83) Sarott, M. F.; Fiebig, M.; Trassin, M. Tracking Ferroelectric Domain Formation during Epitaxial Growth of PbTiO₃ Films. *Appl. Phys. Lett.* **2020**, *117* (13), 132901. <https://doi.org/10.1063/5.0021434>.
- (84) Sarott, M. F.; Rossell, M. D.; Fiebig, M.; Trassin, M. Multilevel Polarization Switching in Ferroelectric Thin Films. *Nat. Commun.* **2022**, *13* (1), 1–7. <https://doi.org/10.1038/s41467-022-30823-5>.
- (85) Puggioni, D.; Giovannetti, G.; Rondinelli, J. M. Polar Metals as Electrodes to Suppress the Critical-Thickness Limit in Ferroelectric Nanocapacitors. *J. Appl. Phys.* **2018**, *124* (17), 174102. <https://doi.org/10.1063/1.5049607>.
- (86) Zeches, R. J.; Rossell, M. D.; Zhang, J. X.; Hatt, A. J.; He, Q.; Yang, C.-H.; Kumar, A.; Wang, C. H.; Melville, A.; Adamo, C.; Sheng, G.; Chu, Y.-H.; Ihlefeld, J. F.; Erni, R.; Ederer, C.; Gopalan, V.; Chen, L. Q.; Schlom, D. G.; Spaldin, N. A.; Martin, L. W.; Ramesh, R. A Strain-Driven Morphotropic Phase Boundary in BiFeO₃. *Science* **2009**, *326* (5955), 977–980. <https://doi.org/10.1126/science.1177046>.
- (87) Nordlander, J.; Maillard, A.; Fiebig, M.; Trassin, M. Emergence of Ferroelectricity at the Morphotropic Phase Boundary of Ultrathin BiFeO₃. *ArXiv* **2020**. <https://doi.org/10.48550/arXiv.2005.09685>.
- (88) Zhang, J. X.; He, Q.; Trassin, M.; Luo, W.; Yi, D.; Rossell, M. D.; Yu, P.; You, L.; Wang, C. H.; Kuo, C. Y.; Heron, J. T.; Hu, Z.; Zeches, R. J.; Lin, H. J.; Tanaka, A.; Chen, C. T.; Tjeng, L. H.; Chu, Y.-H.; Ramesh, R. Microscopic Origin of the Giant Ferroelectric Polarization in Tetragonal-like BiFeO₃. *Phys. Rev. Lett.* **2011**, *107* (14), 147602. <https://doi.org/10.1103/PhysRevLett.107.147602>.
- (89) Seidel, J.; Trassin, M.; Zhang, Y.; Maksymovych, P.; Uhlig, T.; Milde, P.; Köhler, D.; Baddorf, A. P.; Kalinin, S. V.; Eng, L. M.; Pan, X.; Ramesh, R. Electronic Properties of Isosymmetric Phase Boundaries in Highly Strained Ca-Doped BiFeO₃. *Adv. Mater.* **2014**, *26* (25), 4376–4380. <https://doi.org/10.1002/ADMA.201400557>.
- (90) Gattinoni, C.; Strkalj, N.; Härdi, R.; Fiebig, M.; Trassin, M.; Spaldin, N. A. Interface and Surface Stabilization of the Polarization in Ferroelectric Thin Films. *Proc. Natl. Acad. Sci. U. S. A.* **2020**, *117* (46), 28589–28595. <https://doi.org/10.1073/pnas.2007736117>.

- (91) Domingo, N.; Gaponenko, I.; Cordero-Edwards, K.; Stucki, N.; Pérez-Dieste, V.; Escudero, C.; Pach, E.; Verdaguer, A.; Paruch, P. Surface Charged Species and Electrochemistry of Ferroelectric Thin Films. *Nanoscale* **2019**, *11* (38), 17920–17930. <https://doi.org/10.1039/C9NR05526F>.
- (92) Strkalj, N.; Gattinoni, C.; Vogel, A.; Campanini, M.; Haerdi, R.; Rossi, A.; Rossell, M. D.; Spaldin, N. A.; Fiebig, M.; Trassin, M. In-Situ Monitoring of Interface Proximity Effects in Ultrathin Ferroelectrics. *Nat. Commun.* **2020**, *11*, 5815. <https://doi.org/10.1038/s41467-020-19635-7>.
- (93) Chanthbouala, A.; Garcia, V.; Cherifi, R. O.; Bouzehouane, K.; Fusil, S.; Moya, X.; Xavier, S.; Yamada, H.; Deranlot, C.; Mathur, N. D.; Bibes, M.; Barthélémy, A.; Grollier, J. A Ferroelectric Memristor. *Nat. Mater.* **2012**, *11* (10), 860–864. <https://doi.org/10.1038/nmat3415>.
- (94) Agar, J. C.; Mangalam, R. V. K.; Damodaran, A. R.; Velarde, G.; Karthik, J.; Okatan, M. B.; Chen, Z. H.; Jesse, S.; Balke, N.; Kalinin, S. V.; Martin, L. W. Tuning Susceptibility via Misfit Strain in Relaxed Morphotropic Phase Boundary PbZr_{1-x}Ti_xO₃ Epitaxial Thin Films. *Adv. Mater. Interfaces* **2014**, *1* (5), 1400098. <https://doi.org/10.1002/ADMI.201400098>.
- (95) Aurivillius, B. Mixed Bismuth Oxides with Layer Lattices. 1. The Structure Type of CaNb₂Bi₂O₉. *Ark. Kemi.* **1949**, *1*, 463–480.
- (96) A-Paz de Araujo, C.; Cuchiaro, J. D.; McMillian, L. D.; Scott, M. C.; Scott, J. F. Fatigue-Free Ferroelectric Capacitors with Platinum Electrodes. *Nature* **1995**, *374*, 627–629. <https://doi.org/10.1038/374627a0>.
- (97) Keeney, L.; Maity, T.; Schmidt, M.; Amann, A.; Deepak, N.; Petkov, N.; Roy, S.; Pemble, M. E.; Whatmore, R. W. Magnetic Field-Induced Ferroelectric Switching in Multiferroic Aurivillius Phase Thin Films at Room Temperature. **2013**, 2357 (32991). <https://doi.org/10.1111/jace.12467>.
- (98) Keeney, L.; Saghi, Z.; O'Sullivan, M.; Alaria, J.; Schmidt, M.; Colfer, L. Persistence of Ferroelectricity Close to Unit-Cell Thickness in Structurally Disordered Aurivillius Phases. *Chem. Mater.* **2020**, *32* (24), 10511–10523. <https://doi.org/10.1021/acs.chemmater.0c03454>.
- (99) Campanini, M.; Trassin, M.; Ederer, C.; Erni, R.; Rossell, M. D. Buried In-Plane Ferroelectric Domains in Fe-Doped Single-Crystalline Aurivillius Thin Films. *ACS Appl. Electron. Mater.* **2019**, *1* (6), 1019–1028. https://doi.org/10.1021/ACSAELM.9B00180/ASSET/IMAGES/LARGE/EL-2019-00180D_0008.JPEG.
- (100) Gradauskaite, E.; Campanini, M.; Biswas, B.; Schneider, C. W.; Fiebig, M.; Rossell, M. D.; Trassin, M. Robust In-Plane Ferroelectricity in Ultrathin Epitaxial Aurivillius Films. *Adv. Mater. Interfaces* **2020**, *7* (14), 2000202. <https://doi.org/10.1002/admi.202000202>.
- (101) Gradauskaite, E.; Gray, N.; Campanini, M.; Rossell, M. D.; Trassin, M. Nanoscale Design of High-Quality Epitaxial Aurivillius Thin Films. *Chem. Mater.* **2021**, *33* (23), 9439–9446. <https://doi.org/10.1021/acs.chemmater.1c03466>.
- (102) Keeney, L.; Smith, R. J.; Palizdar, M.; Schmidt, M.; Bell, A. J.; Coleman, J. N.; Whatmore, R. W. Ferroelectric Behavior in Exfoliated 2D Aurivillius Oxide

- Flakes of Sub-Unit Cell Thickness. *Adv. Electron. Mater.* **2020**, *6*, 1901264. <https://doi.org/10.1002/aelm.201901264>.
- (103) Gradauskaite, E.; Meier, Q. N.; Gray, N.; Campanini, M.; Moran, T.; Huey, B. D.; Rossell, M. D.; Fiebig, M.; Trassin, M. Defeating Depolarizing Fields with Artificial Flux Closure in Ultrathin Ferroelectrics. **2022**. <https://doi.org/10.48550/arXiv.2212.11073>.
- (104) Wu, M.; Li, J. Sliding Ferroelectricity in 2D van Der Waals Materials: Related Physics and Future Opportunities. *Proc. Natl. Acad. Sci. U. S. A.* **2021**, *118* (50), 1–9. <https://doi.org/10.1073/pnas.2115703118>.
- (105) Tsymbal, E. Y. Two-Dimensional Ferroelectricity by Design. *Science (80-)*. **2021**, *372* (6549), 1389–1390. <https://doi.org/10.1126/science.abi7296>.
- (106) Oltmans, S. J.; Lelieveld, J.; Tost, H.; Glatthor, N.; Bhartia, P. K.; Haffner, D.; Labow, G. L.; Flynn, L.; Weber, M.; Burrows, J. P.; Pan, L. L.; Konopka, P.; Kinnison, D. E.; Tilmes, S.; Kinnison, D.; Bandoro, J.; Garcia, R. R.; Nash, E. R.; Kawa, S. R.; Montzka, S. A.; Schauffler, S. M.; Freckleton, R. S.; Shine, K. P.; Bodeker, G. E.; Solomon, S.; Young, P. J.; Drdla, K.; Schoeberl, M. R.; Hamill, P.; Toon, O. B.; Abalichin, J.; Langematz, U.; Austin, J.; Wilson, J.; Shepherd, T. G. Discovery of Robust In-Plane Ferroelectricity in Atomic-Thick SnTe. *Science (80-)*. **2016**, *353* (6296), 274–278.
- (107) Yuan, S.; Luo, X.; Chan, H. L.; Xiao, C.; Dai, Y.; Xie, M.; Hao, J. Room-Temperature Ferroelectricity in MoTe₂ down to the Atomic Monolayer Limit. *Nat. Commun.* **2019**, *10* (1), 2–7. <https://doi.org/10.1038/s41467-019-09669-x>.
- (108) Ding, W.; Zhu, J.; Wang, Z.; Gao, Y.; Xiao, D.; Gu, Y.; Zhang, Z.; Zhu, W. Prediction of Intrinsic Two-Dimensional Ferroelectrics in In₂Se₃ and Other III₂-VI₃ van Der Waals Materials. *Nat. Commun.* **2017**, *8*, 1–8. <https://doi.org/10.1038/ncomms14956>.
- (109) Belianinov, A.; He, Q.; Dziaugys, A.; Maksymovych, P.; Eliseev, E.; Borisevich, A.; Morozovska, A.; Banys, J.; Vysochanskii, Y.; Kalinin, S. V. CuInP₂S₆ Room Temperature Layered Ferroelectric. *Nano Lett.* **2015**, *15* (6), 3808–3814. <https://doi.org/10.1021/acs.nanolett.5b00491>.
- (110) Zheng, Z.; Ma, Q.; Bi, Z.; de la Barrera, S.; Liu, M. H.; Mao, N.; Zhang, Y.; Kiper, N.; Watanabe, K.; Taniguchi, T.; Kong, J.; Tisdale, W. A.; Ashoori, R.; Gedik, N.; Fu, L.; Xu, S. Y.; Jarillo-Herrero, P. Unconventional Ferroelectricity in Moiré Heterostructures. *Nature* **2020**, *588* (7836), 71–76. <https://doi.org/10.1038/s41586-020-2970-9>.
- (111) Vizner Stern, M.; Waschitz, Y.; Cao, W.; Nevo, I.; Watanabe, K.; Taniguchi, T.; Sela, E.; Urbakh, M.; Hod, O.; Ben Shalom, M. Interfacial Ferroelectricity by van Der Waals Sliding. *Science (80-)*. **2021**, *372* (6549), 142–1466. <https://doi.org/10.1126/science.abe8177>.
- (112) Miao, L.; Ding, N.; Wang, N.; Shi, C.; Ye, H.; Li, L. Direct Observation of Geometric and Sliding Ferroelectricity in an Amphidynamic Crystal. *Nat. Mater.* **2022**. <https://doi.org/10.1038/s41563-022-01322-1>.
- (113) Wang, X.; Yasuda, K.; Zhang, Y.; Liu, S.; Watanabe, K.; Taniguchi, T.; Hone, J.; Fu, L.; Jarillo-Herrero, P. Interfacial Ferroelectricity in Rhombohedral-Stacked Bilayer Transition Metal Dichalcogenides. *Nat. Nanotechnol.* **2022**, *17*

- (4), 367–371. <https://doi.org/10.1038/s41565-021-01059-z>.
- (114) Chandrasekaran, A.; Mishra, A.; Singh, A. K. Ferroelectricity, Antiferroelectricity, and Ultrathin 2D Electron/Hole Gas in Multifunctional Monolayer MXene. *Nano Lett.* **2017**, *17* (5), 3290–3296. <https://doi.org/10.1021/acs.nanolett.7b01035>.
- (115) Böscke, T. S.; Müller, J.; Bräuhäus, D.; Schröder, U.; Böttger, U. Ferroelectricity in Hafnium Oxide Thin Films. *Appl. Phys. Lett.* **2011**, *99* (10). <https://doi.org/10.1063/1.3634052>.
- (116) Robertson, J. High Dielectric Constant Oxides. *Eur. Phys. J. Appl. Phys.* **2004**, *28* (3), 265–291. <https://doi.org/10.1051/epjap:2004206>.
- (117) Hyuk Park, M.; Joon Kim, H.; Jin Kim, Y.; Lee, W.; Moon, T.; Seong Hwang, C. Evolution of Phases and Ferroelectric Properties of Thin Hf_{0.5}Zr_{0.5}O₂ Films According to the Thickness and Annealing Temperature. *Appl. Phys. Lett.* **2013**, *102* (24), 242905. <https://doi.org/10.1063/1.4811483>.
- (118) Cheema, S. S.; Shanker, N.; Hsu, S. L.; Rho, Y.; Hsu, C. H.; Stoica, V. A.; Zhang, Z.; Freeland, J. W.; Shafer, P.; Grigoropoulos, C. P.; Ciston, J.; Salahuddin, S. Emergent Ferroelectricity in Subnanometer Binary Oxide Films on Silicon. *Science (80-)*. **2022**, *376* (6593), 648–652. <https://doi.org/10.1126/science.abm8642>.
- (119) Schroeder, U.; Park, M. H.; Mikolajick, T.; Hwang, C. S. The Fundamentals and Applications of Ferroelectric HfO₂. *Nat. Rev. Mater.* **2022**, *0123456789*. <https://doi.org/10.1038/s41578-022-00431-2>.
- (120) Cheema, S. S.; Kwon, D.; Shanker, N.; dos Reis, R.; Hsu, S. L.; Xiao, J.; Zhang, H.; Wagner, R.; Datar, A.; McCarter, M. R.; Serrao, C. R.; Yadav, A. K.; Karbasian, G.; Hsu, C. H.; Tan, A. J.; Wang, L. C.; Thakare, V.; Zhang, X.; Mehta, A.; Karapetrova, E.; Chopdekar, R. V.; Shafer, P.; Arenholz, E.; Hu, C.; Proksch, R.; Ramesh, R.; Ciston, J.; Salahuddin, S. Enhanced Ferroelectricity in Ultrathin Films Grown Directly on Silicon. *Nature* **2020**, *580* (7804), 478–482. <https://doi.org/10.1038/s41586-020-2208-x>.
- (121) Nukala, P.; Ahmadi, M.; Wei, Y.; Graaf, S. De; Stylianidis, E.; Chakraborty, T.; Matzen, S.; Zandbergen, H. W.; Björling, A.; Mannix, D.; Carbone, D.; Kooi, B.; Noheda, B. Reversible Oxygen Migration and Phase Transitions in Hafnia-Based Ferroelectric Devices. *Science (80-)*. **2021**, *372* (6542), 630–635. <https://doi.org/10.1126/science.abf3789>.
- (122) Zhou, S.; Zhang, J.; Rappe, A. M. Strain-Induced Antipolar Phase in Hafnia Stabilizes Robust Thin-Film Ferroelectricity. *Sci. Adv.* **2022**, *8* (47), eadd5953. <https://doi.org/10.1126/sciadv.add5953>.
- (123) Cheema, S. S.; Shanker, N.; Wang, L. C.; Hsu, C. H.; Hsu, S. L.; Liao, Y. H.; San Jose, M.; Gomez, J.; Chakraborty, W.; Li, W.; Bae, J. H.; Volkman, S. K.; Kwon, D.; Rho, Y.; Pinelli, G.; Rastogi, R.; Pipitone, D.; Stull, C.; Cook, M.; Tyrrell, B.; Stoica, V. A.; Zhang, Z.; Freeland, J. W.; Tassone, C. J.; Mehta, A.; Saheli, G.; Thompson, D.; Suh, D. I.; Koo, W. T.; Nam, K. J.; Jung, D. J.; Song, W. Bin; Lin, C. H.; Nam, S.; Heo, J.; Parihar, N.; Grigoropoulos, C. P.; Shafer, P.; Fay, P.; Ramesh, R.; Mahapatra, S.; Ciston, J.; Datta, S.; Mohamed, M.; Hu, C.; Salahuddin, S. Ultrathin Ferroic HfO₂–ZrO₂ Superlattice Gate Stack for

- Advanced Transistors. *Nature* **2022**, *604* (7904), 65–71.
<https://doi.org/10.1038/s41586-022-04425-6>.
- (124) Ihlefeld, J. F.; Luk, T. S.; Smith, S. W.; Fields, S. S.; Jaszewski, S. T.; Hirt, D. M.; Riffe, W. T.; Bender, S.; Constantin, C.; Ayyasamy, M. V.; Balachandran, P. V.; Lu, P.; David Henry, M.; Davids, P. S. Compositional Dependence of Linear and Nonlinear Optical Response in Crystalline Hafnium Zirconium Oxide Thin Films. *J. Appl. Phys.* **2020**, *128* (3), 034101. <https://doi.org/10.1063/5.0012175>.
- (125) Cheema, S. S.; Kwon, D.; Shanker, N.; dos Reis, R.; Hsu, S. L.; Xiao, J.; Zhang, H.; Wagner, R.; Datar, A.; McCarter, M. R.; Serrao, C. R.; Yadav, A. K.; Karbasian, G.; Hsu, C. H.; Tan, A. J.; Wang, L. C.; Thakare, V.; Zhang, X.; Mehta, A.; Karapetrova, E.; Chopdekar, R. V.; Shafer, P.; Arenholz, E.; Hu, C.; Proksch, R.; Ramesh, R.; Ciston, J.; Salahuddin, S. Enhanced Ferroelectricity in Ultrathin Films Grown Directly on Silicon. *Nature* **2020**, *580* (7804), 478–482. <https://doi.org/10.1038/s41586-020-2208-x>.
- (126) Qin, J.; Huang, F.; Li, X.; Deng, L.; Kang, T.; Markov, A.; Yue, F.; Chen, Y.; Wen, X.; Liu, S.; Xiong, Q.; Semin, S.; Rasing, T.; Modotto, D.; Morandotti, R.; Xu, J.; Duan, H.; Bi, L. Enhanced Second Harmonic Generation from Ferroelectric HfO₂-Based Hybrid Metasurfaces. *ACS Nano* **2019**, *13* (2), 1213–1222. <https://doi.org/10.1021/acsnano.8b06308>.
- (127) Spaldin, N. A.; Efe, I.; Rossell, M. D.; Gattinoni, C. Layer and Spontaneous Polarizations in Perovskite Oxides and Their Interplay in Multiferroic Bismuth Ferrite. *J. Chem. Phys.* **2021**, *154* (15), 154702. <https://doi.org/10.1063/5.0046061>.
- (128) Efe, I.; Spaldin, N. A.; Gattinoni, C. On the Happiness of Ferroelectric Surfaces and Its Role in Water Dissociation: The Example of Bismuth Ferrite. *J. Chem. Phys.* **2021**, *154* (2), 024702. <https://doi.org/10.1063/5.0033897>.
- (129) Gattinoni, C.; Spaldin, N. A. Prediction of a Strong Polarizing Field in Thin Film Paraelectrics. *Phys. Rev. Res.* **2022**, *4* (3), L032020. <https://doi.org/10.1103/PHYSREVRSEARCH.4.L032020/FIGURES/4/MEDIUM>.
- (130) Fusil, S.; Chauleau, J.-Y.; Li, X.; Fischer, J.; Dufour, P.; Léveillé, C.; Carrétéro, C.; Jaouen, N.; Viret, M.; Gloter, A.; Garcia, V. Polar Chirality in BiFeO₃ Emerging from A Peculiar Domain Wall Sequence. *Adv. Electron. Mater.* **2022**, 2101155. <https://doi.org/10.1002/AELM.202101155>.
- (131) Das, S.; Hong, Z.; McCarter, M.; Shafer, P.; Shao, Y. T.; Muller, D. A.; Martin, L. W.; Ramesh, R. A New Era in Ferroelectrics. *APL Mater.* **2020**, *8* (12), 120902. <https://doi.org/10.1063/5.0034914>.
- (132) Phuong Dao, T.; Müller, M.; Luo, Z.; Baumgartner, M.; Hrabec, A.; Heyderman, L. J.; Gambardella, P. Chiral Domain Wall Injector Driven by Spin-Orbit Torques. *Nano Lett.* **2019**, *19* (9), 5930–5937. https://doi.org/10.1021/ACS.NANOLETT.9B01504/ASSET/IMAGES/LARGE/NL9B01504_0004.JPEG.
- (133) Vélez, S.; Ruiz-gómez, S.; Schaab, J.; Gradauskaite, E.; Wörnle, M. S.; Welter, P.; Jacot, B. J.; Degen, C. L.; Trassin, M.; Fiebig, M.; Gambardella, P. Current-Driven Dynamics and Ratchet Effect of Skyrmion Bubbles in a Ferrimagnetic

Insulator. *Nat. Nanotechnol.* **2022**. <https://doi.org/10.1038/s41565-022-01144-x>.

- (134) Vélez, S.; Schaab, J.; Wörnle, M. S.; Müller, M.; Gradauskaite, E.; Welter, P.; Gutgsell, C.; Nistor, C.; Degen, C. L.; Trassin, M.; Fiebig, M.; Gambardella, P. High-Speed Domain Wall Racetracks in a Magnetic Insulator. *Nat. Commun.* **2019**, *10*, 4750.
- (135) Dzyaloshinskii, I. E. Theory of Helicoidal Structures in Antiferromagnets. I. Nonmetals. *Jetp* **1964**, *19* (4), 960–971.
- (136) Goncalves, M. A. P.; Escorihuela-Sayalero, C.; Garcia-Fernandez, P.; Junquera, J.; Iniguez, J. Theoretical Guidelines to Create and Tune Electric Skyrmions. *Sci. Adv.* **2019**, *5*, eaau7023.
- (137) Bousquet, E.; Dawber, M.; Stucki, N.; Lichtensteiger, C.; Hermet, P.; Gariglio, S.; Triscone, J. M.; Ghosez, P. Improper Ferroelectricity in Perovskite Oxide Artificial Superlattices. *Nature* **2008**, *452* (7188), 732–736. <https://doi.org/10.1038/nature06817>.
- (138) Chauleau, J.-Y.; Chirac, T.; Fusil, S.; Garcia, V.; Akhtar, W.; Tranchida, J.; Thibaudeau, P.; Gross, I.; Blouzon, C.; Finco, A.; Bibes, M.; Dkhil, B.; Khalyavin, D. D.; Manuel, P.; Jacques, V.; Jaouen, N.; Viret, M. Electric and Antiferromagnetic Chiral Textures at Multiferroic Domain Walls. *Nat. Mater.* **2019**, 1–5. <https://doi.org/10.1038/s41563-019-0516-z>.